Structural Consequences of β-Amino Acid Preorganization in a Self-Assembling α/β-Peptide: Fundamental Studies of Foldameric Helix Bundles

*Joshua L. Price, W. Seth Horne, and Samuel H. Gellman**

Department of Chemistry, University of Wisconsin, Madison, WI 53706

Supporting Information

Table of Contents

Peptide Synthesis **S2**
General S2
Synthesis of α/β-peptide **3** S2
Synthesis of α/β-peptides **4**–**10** S3
Cleavage and purification S4
Purification and Characterization S5
MALDI S6
HPLC S15
Circular Dichroism Spectroscopy **S20**
Analytical Ultracentrifugation **S20**
X-ray Crystallography **S34**
Analysis of Backbone Dihedral Angles in α/β-Peptides **5**-**10** S37
Analysis of Structural Differences Between α/β-Peptide **6** and α/β-Peptides **1**, **5**, **7**-**10** S38
Summary of the Helical Stammer Observed Previously for α/β-Peptide **2** S39
References **S41**

Peptide Synthesis

General

Peptides were synthesized on solid phase using standard Fmoc chemistry. Amino acids were activated by 2-(1H-benzotriazole-1-yl)-1,1,3,3-tetramethyluronium hexafluorophosphate (HBTU, purchased from Anaspec) and N-hydroxybenzotriazole (HOBt, purchased from Aldrich). Fmoc-Arg(Pbf) loaded Novasyn TGA resin and all Fmoc-protected α-amino acids with acid-labile side-chain protecting groups were purchased from Novabiochem. Fmoc-ACPC[1] and Fmoc-APC(Boc)[2] were synthesized as described previously. Fmoc-protected β^3-amino acids were purchased from Peptech. We thank Peptech for providing these Fmoc-protected β^3-amino acids at a discounted price. N,N-dimethylformamide (DMF) and N-methyl morpholine (NMM) were purchased from Aldrich.

Synthesis of α/β-peptide 3

α/β-Peptide **3** was synthesized as the C-terminal acid on solid phase using microwave-assisted peptide synthesis.[3,4] A general procedure follows: NovaSyn TGA resin (25 μmol, bearing Fmoc-Arg(Pbf)) was weighed into a fritted polypropylene tube and allowed to swell first in CH_2Cl_2, then in DMF. To remove the Fmoc group from the amine on the resin-bound amino acid, 3 mL of 20% piperidine in DMF was added to the resin, and the resin was heated to 80 °C in a MARS V multimode microwave (2 minute ramp to 80 °C, 2 minute hold at 80 °C) with stirring. Following the deprotection reaction, the resin was washed with DMF (3×).

For coupling of an activated amino acid to an unprotected amine on resin, the desired Fmoc-protected amino acid (125 μmol, 5 eq) and HBTU (47 mg, 125 μmol, 5 eq) were

dissolved by vortexing in 1250 μl of 0.1 M HOBt in DMF (125 μmol HOBt, 5 eq). To this solution was added 55 μl N-methyl morpholine (NMM, 500 μL, 20 eq). The resulting mixture was vortexed briefly, and allowed to react for at least 1 min. The activated amino acid solution was then added to the fritted polypropylene tube containing the resin. The resin was heated to 70 °C in the microwave (2 minute ramp to 70 °C, 4 minute hold at 70 °C) with stirring.

Following the coupling reaction, the resin was removed from the microwave, the activated amino acid solution was drained from the resin with a vacuum manifold, and the resin was washed with DMF (3×). The deprotection and coupling cycles were alternately repeated to give the desired full-length peptide. Following the final deprotection cycle, the N-terminal amine was acetylated by stirring the resin in a 14:5:1 mixture of CH_2Cl_2 / acetic anhydride / triethylamine. The resin was washed thoroughly (3× DMF, 3× CH_2Cl_2, and 3× MeOH) and then dried under vacuum. Cleavage and purification are described below.

Synthesis of α/β-peptides 4–10

α/β-Peptides **4**–**10** were prepared as C-terminal acids on solid phase via a combination of manual and automated peptide synthesis methods. A general procedure follows: Fmoc-Arg(Pbf) loaded NovaSyn TGA resin (125 mg, 25 μmol; mass of resin used depends on resin loading, which is usually near 0.2 mmol/g) was weighed into a fritted polypropylene tube and allowed to swell first in CH_2Cl_2, then in DMF. To remove the Fmoc group from the amine on the resin-bound amino acid, 20% piperidine in DMF (3 mL) was added to the resin; the polypropylene tube was capped and allowed to agitate on a bench top shaker for 15 min. Following the deprotection reaction, the resin was washed with DMF (3×).

Fmoc-amino acid (125 μmol, 5 eq) and HBTU (47 mg, 125 μmol, 5 eq) were weighed into a separate tube and dissolved by vortexing in 1250 μl of 0.1 M HOBt in DMF (125 μmol HOBt, 5 eq). To this solution was added 55 μl N-methyl morpholine (NMM, 500 μL, 20 eq). The resulting mixture was vortexed briefly, and allowed to react for at least 1 min. The activated amino acid solution was then added to the fritted polypropylene tube containing the resin, the tube was capped, and the resin was agitated on a bench top shaker for 1 h. The resin was washed with DMF (3×) and the deprotection/coupling cycle was repeated for the next residue. After the second deprotection/coupling cycle, the resin was transferred to an Applied Biosystems Synergy 432A automated peptide synthesizer on which the remaining 30 residues were coupled. The N-terminal amine was acetylated by stirring the resin in a 14:5:1 mixture of CH_2Cl_2 / acetic anhydride / triethylamine. The resin was washed thoroughly (3× DMF, 3× CH_2Cl_2, and 3× MeOH) and then dried under vacuum. Cleavage and purification are described below.

Cleavage and purification

Peptides were globally deprotected and cleaved from the resin by stirring the resin in 95% trifluoroacetic acid (TFA), 2.5% water, and 2.5% triisopropylsilane for 2 to 4 hours. Following the cleavage reaction, the TFA solution was drained from the resin, the resin was rinsed with additional TFA, and the resulting solution was concentrated under N_2. Peptides were precipitated from the concentrated TFA solution by addition of diethyl ether (~45 mL). Following centrifugation, the ether was decanted, and the peptide pellet was washed with diethyl ether. The washed peptide pellet was dried under N_2 and stored at -20 °C until purification.

Purification and Characterization

Immediately prior to purification, the crude peptide was dissolved in 1:1 water:acetonitrile. Peptides were purified by preparative reverse-phase HPLC on a C18 column using a linear gradient of water and acetonitrile with 0.1% v/v TFA. HPLC fractions containing the desired peptide product were pooled, frozen, and lyophilized. Peptides were identified by matrix-assisted laser desorption/ionization time-of-flight spectrometry (MALDI-TOF, Table S1; MALDI spectra appear below in Figure S1–S8), and purity was analyzed by HPLC (Figures S9–S16)

Table S1 ααβ^3-Peptide Sequences and MALDI data[a]

	Name	Peptide Sequence	Calculated $[M+H]^+$ ($g \cdot mol^{-1}$)	Observed $[M+H]^+$ ($g \cdot mol^{-1}$)
		*g**a**bcd**efga**bcd**efga**bcd**efga**bcd**efga*		
1		Ac-RMKQIEDKIEEILSKLYHIENELARIKKLIGER-OH[b]		
2		Ac-(Z)(X)···(X)·····(X)(X)···(Z)·····-OH[b]		
3		Ac-(Z)(X)(X)(X)(X)·····(X)(Z)(Z)(X)-OH	3997.3	3998.6
4		Ac-(X)·····-OH	4201.5	4200.7
5		Ac-·····(X)·····-OH	4200.5	4200.7
6		Ac-·····(X)·····-OH	4216.4	4216.4
7		Ac-·····(X)·····-OH	4216.4	4216.7
8		Ac-·····(X)·····-OH	4200.5	4200.9
9		Ac-(Z)(X)·····(X)·····(Z)·····-OH	4097.3	4097.7
10		Ac-(Z)(X)···(X)·····(X)·····(Z)·····-OH	4065.3	4065.2
		1 5 10 15 20 25 30		

[a]Hydrophobic *a*- and *d*- position residues are highlighted in boldface type. α-Amino acid residues are abbreviated according to the standard one letter code. β^3-Amino acids are highlighted with blue circles and abbreviated with the letter that corresponds to the a-amino acid that bears the same side-chain (according to the standard one letter code). Cyclic β-amino acids are highlighted with red circles and are abbreviated as follows: X = ACPC, Z = APC.

[b]MALDI characterization for these compounds were reported in reference 5

MALDI

MALDI spectra for α/β-peptides **3**–**10** are shown in Figures S1–S8.

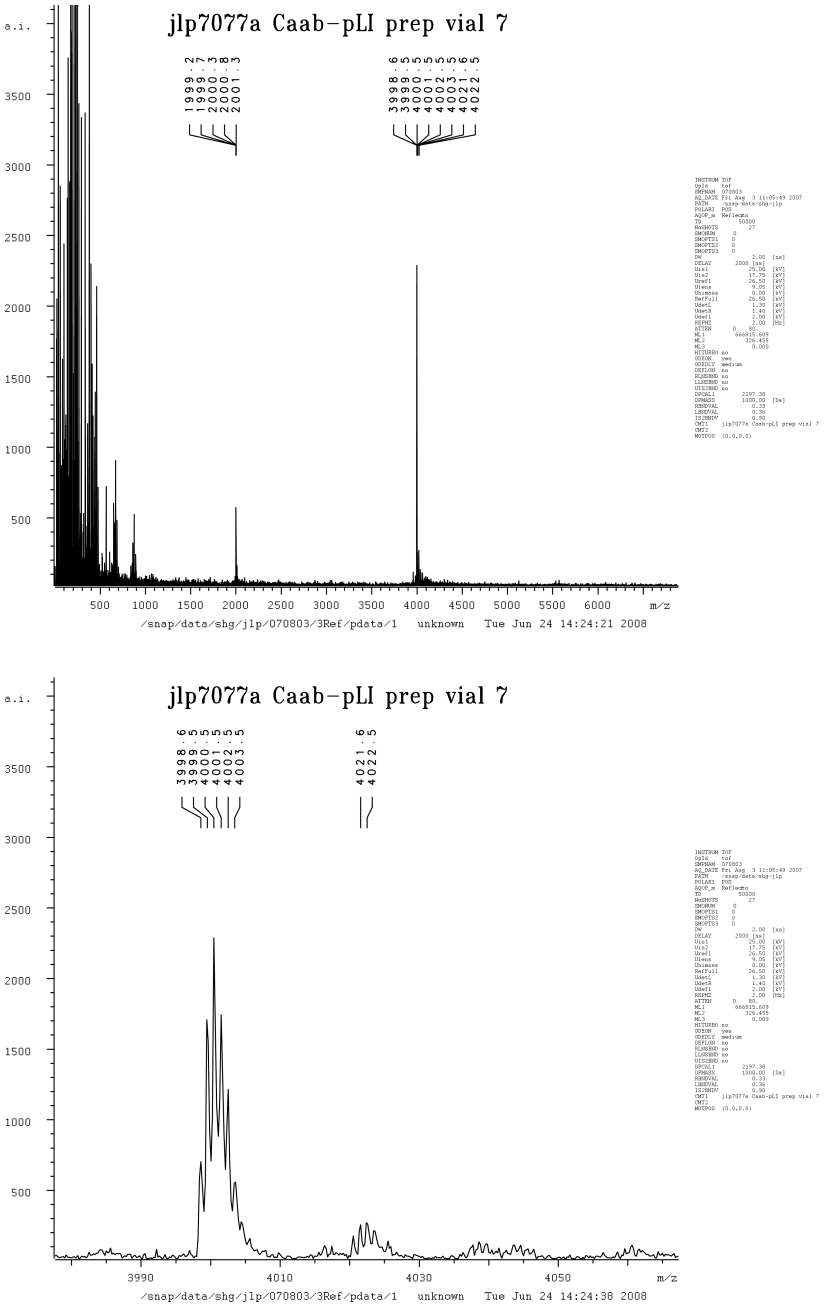

Figure S1. MALDI-TOF spectra for α/β-peptide **3**.

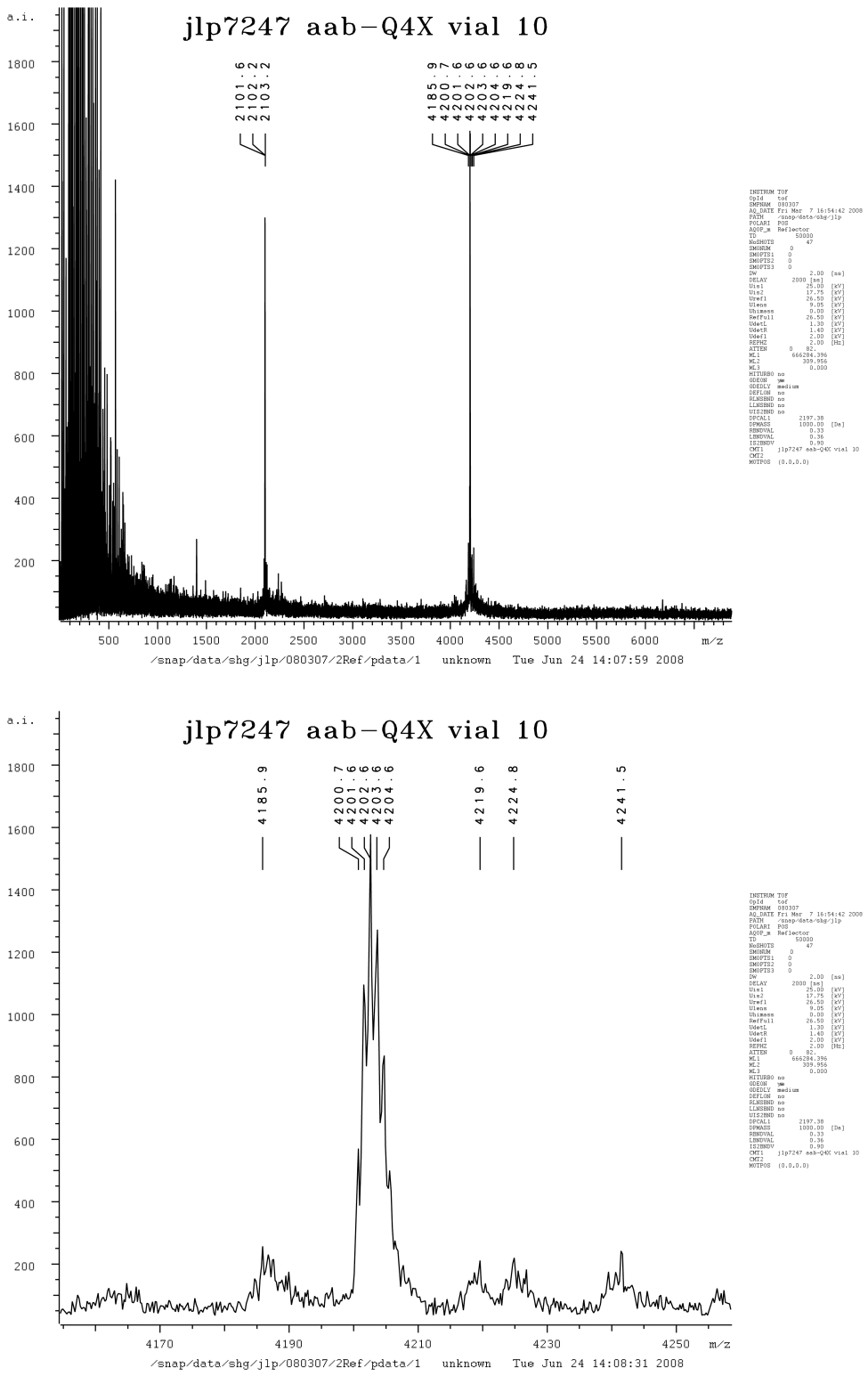

Figure S2. MALDI-TOF spectra for α/β-peptide **4**.

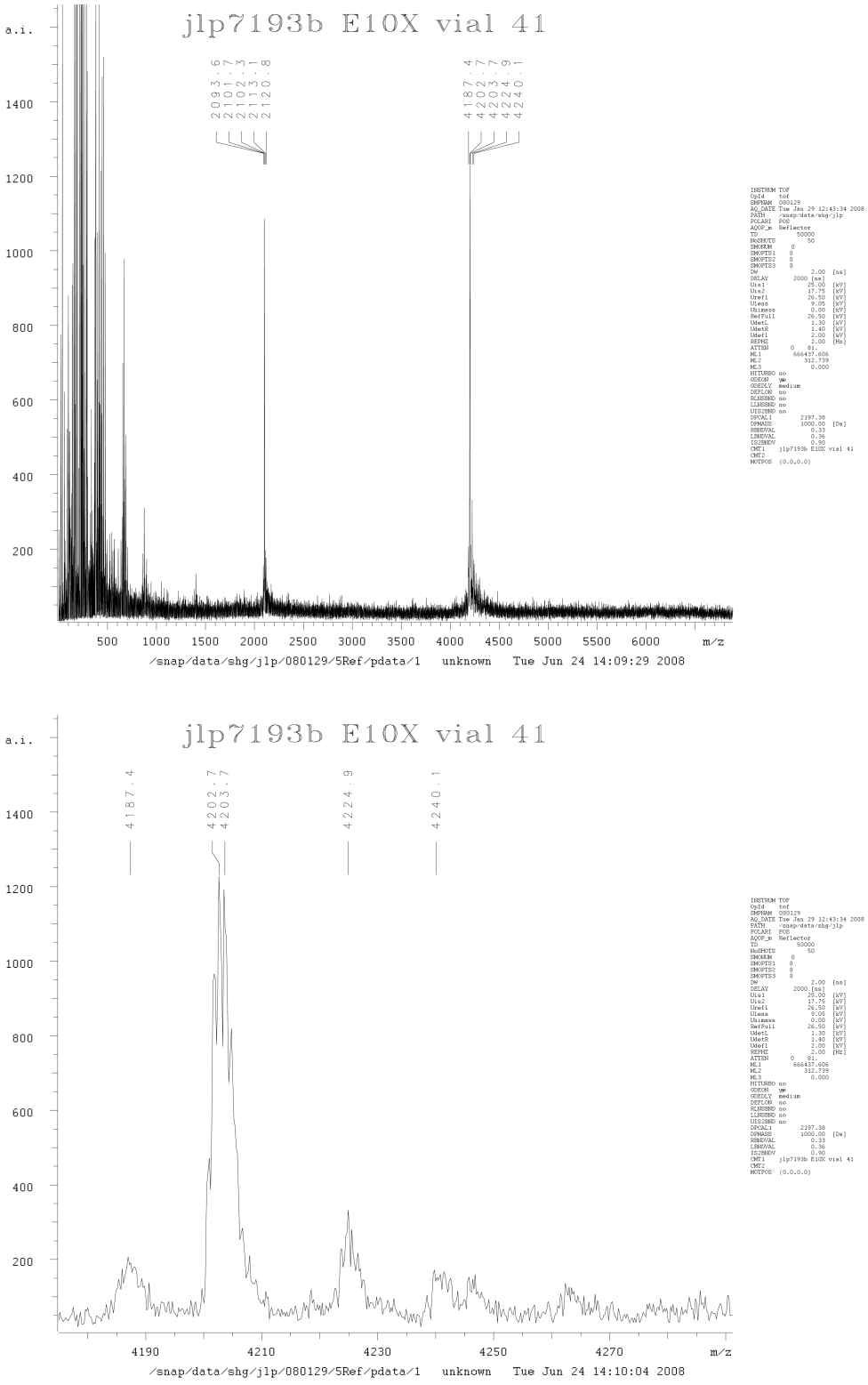

Figure S3. MALDI-TOF spectra for α/β-peptide **5**.

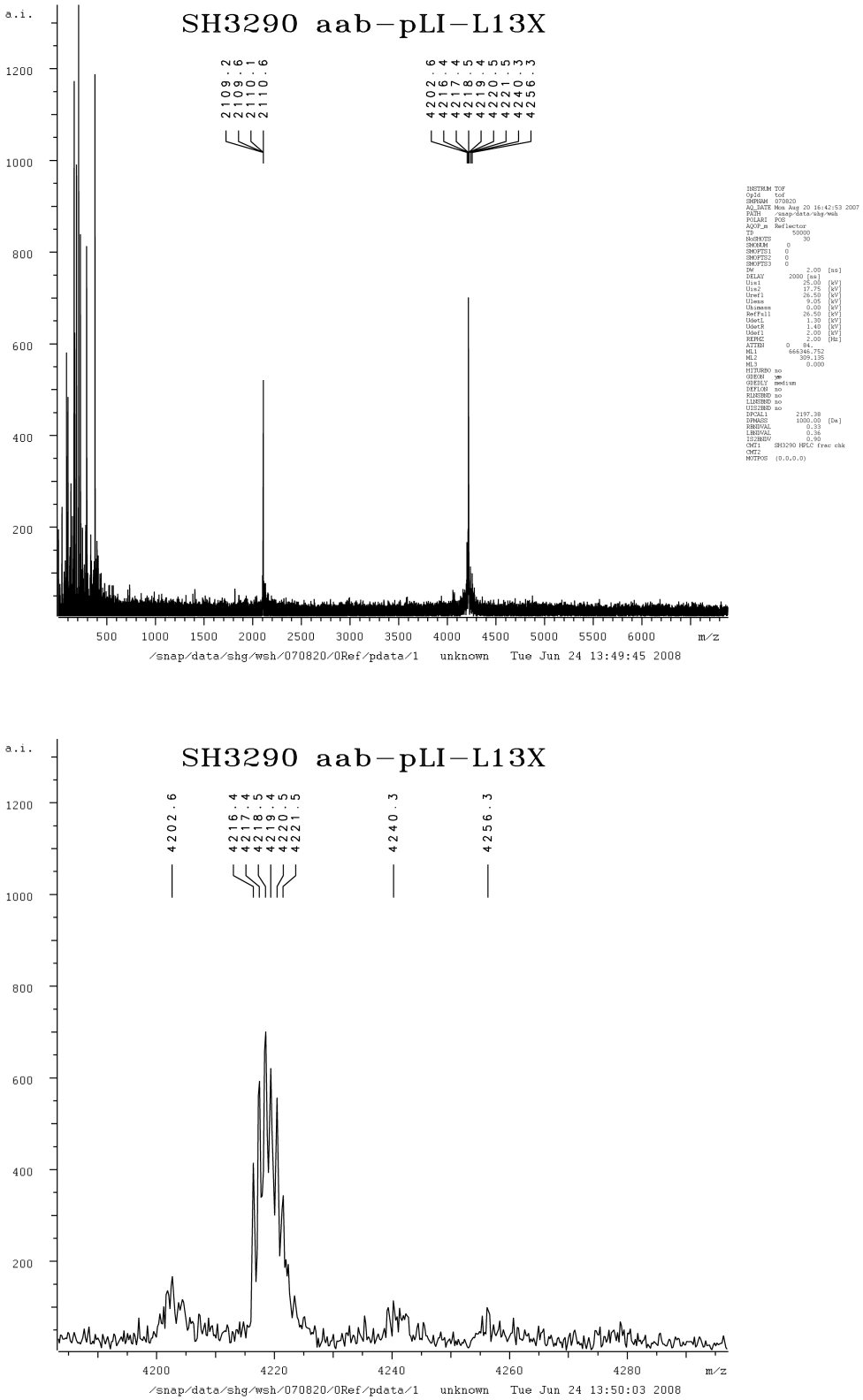

Figure S4. MALDI-TOF spectra for α/β-peptide **6**.

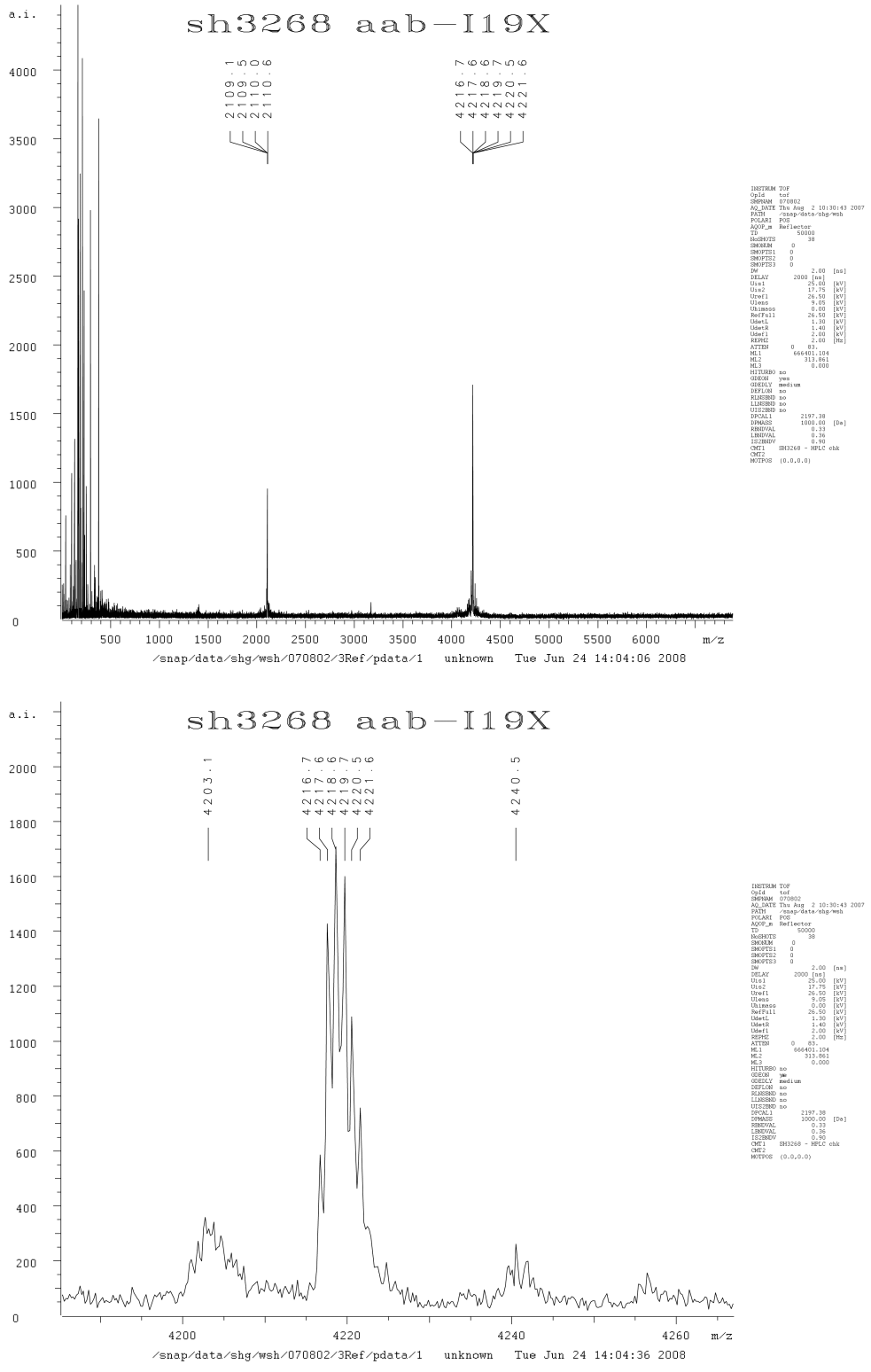

Figure S5. MALDI-TOF spectra for α/β-peptide **7**.

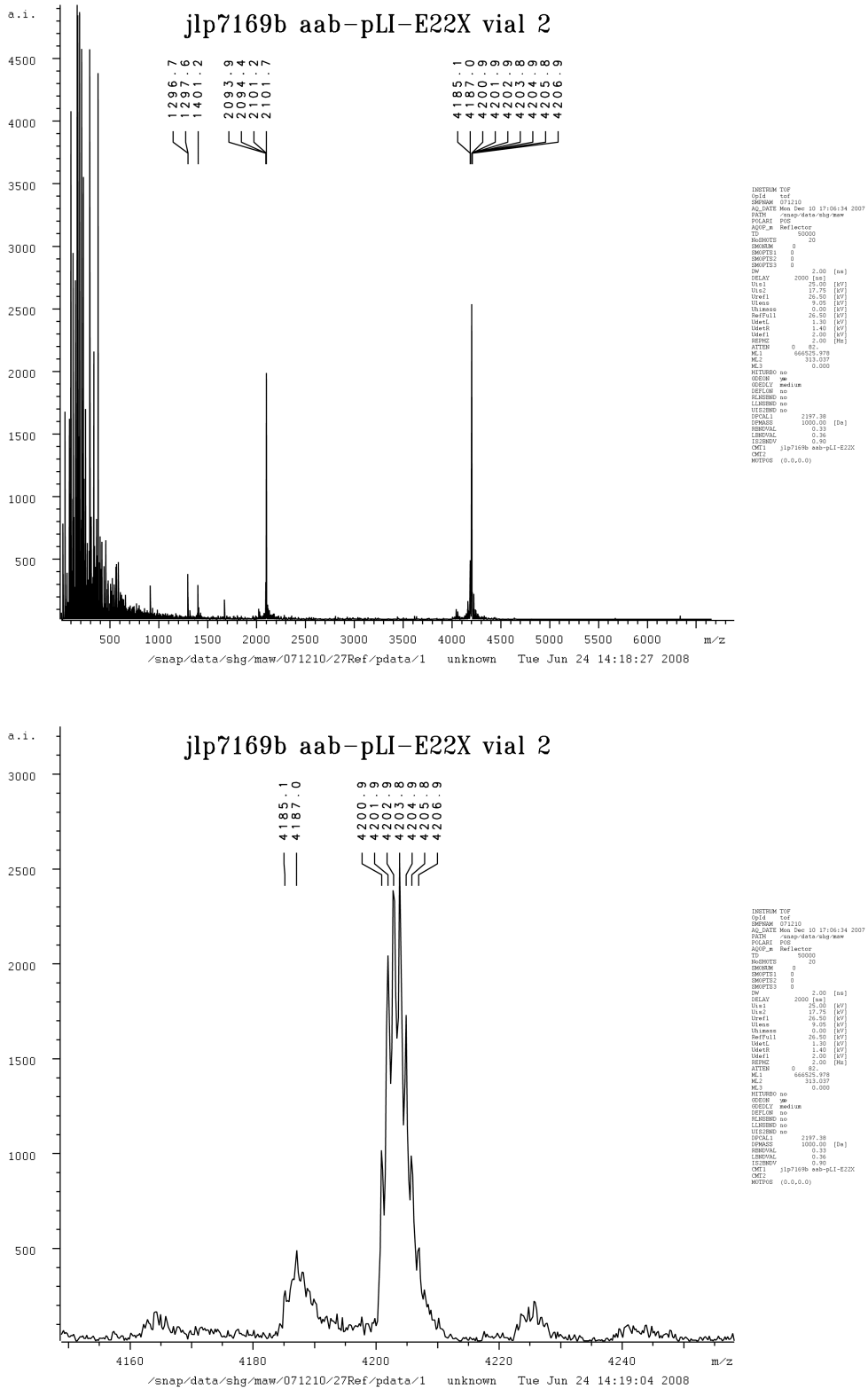

Figure S6. MALDI-TOF spectra for α/β-peptide **8**.

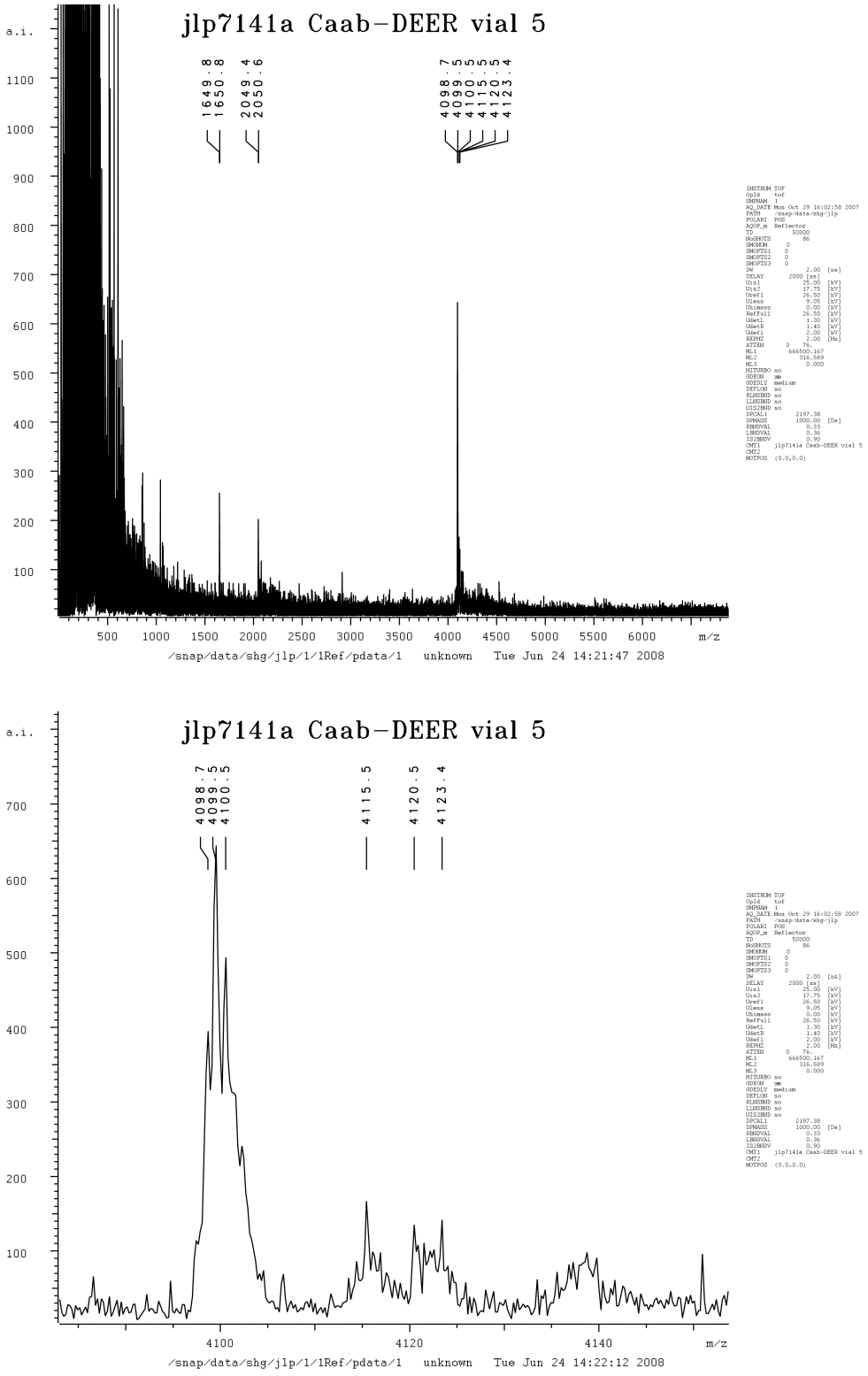

Figure S7. MALDI-TOF spectra for α/β-peptide **9**.

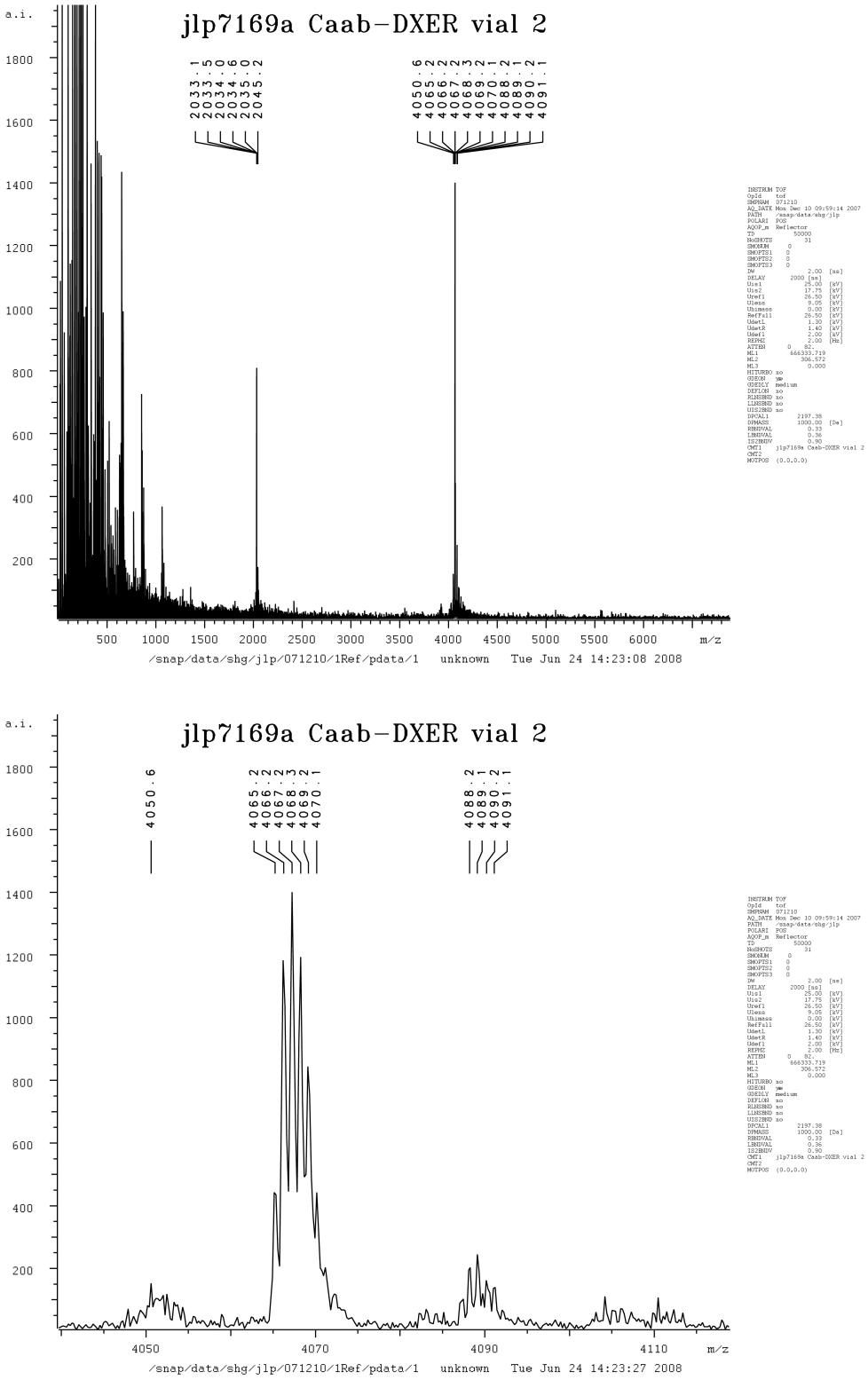

Figure S8. MALDI-TOF spectra for α/β-peptide **10**.

HPLC

HPLC traces for α/β-peptides **3**–**10** are shown in Figures S9–S16.

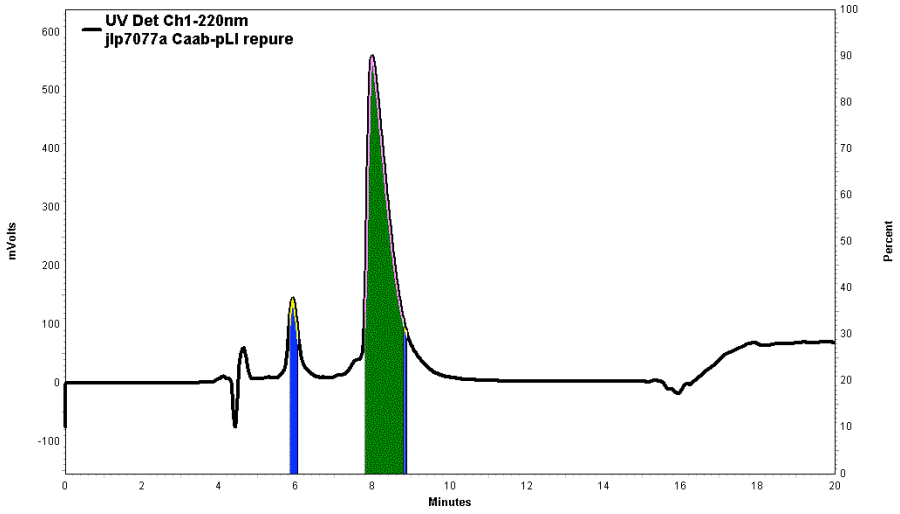

Figure S9. HPLC data for α/β-peptide **3**, showing a representative trace from the repurification of **3**. Peptide solution was injected onto a C18 sempreparative column and eluted using a linear gradient of 44.5–47% acetonitrile in water (constant 0.1% TFA) over 10 minutes. A small amount of an impurity elutes before the desired product. The desired product is collected separately, and should not be contaminated with the earlier impurity.

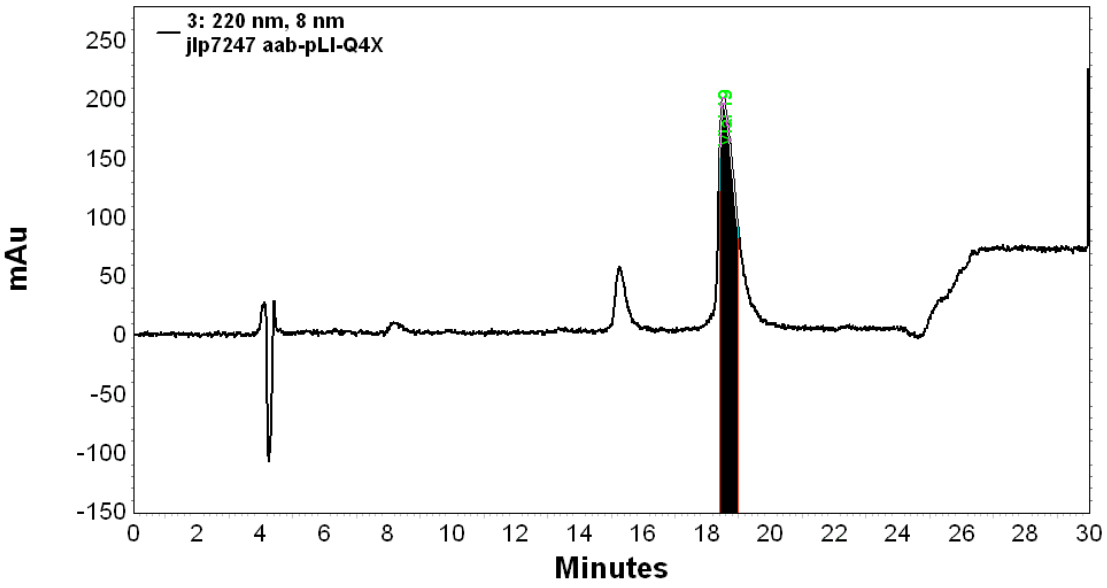

Figure S10. HPLC data for α/β-peptide **4**, showing a representative trace from the repurification of **4**. Peptide solution was injected onto a C18 semipreparative column and eluted using a linear gradient of 44-54% acetonitrile in water (constant 0.1% TFA) over 20 minutes. A small amount of impurity elutes before the desired product, but should be removed from the final product.

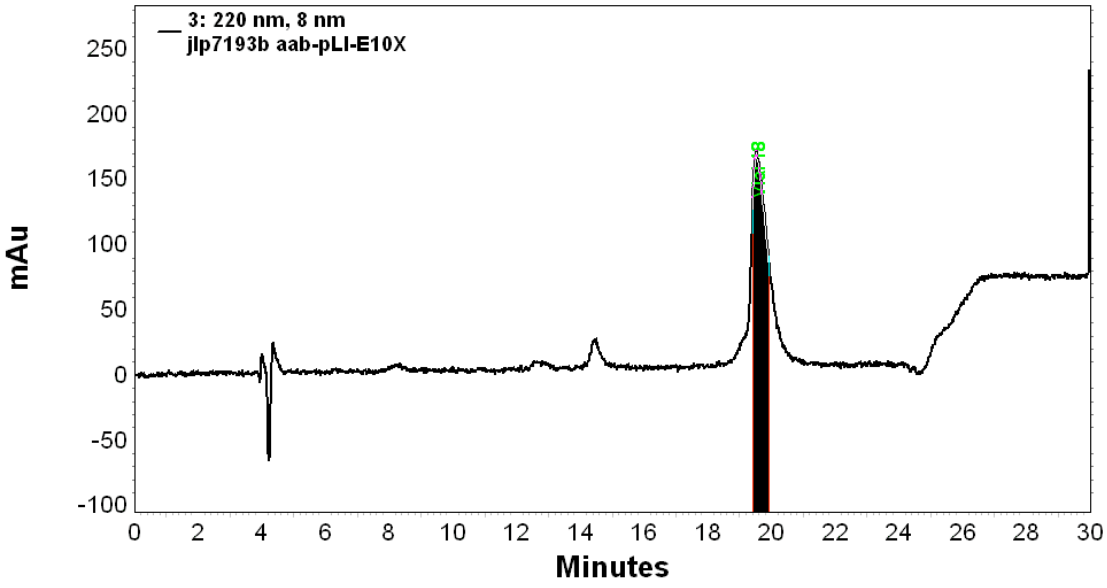

Figure S11. HPLC data for α/β-peptide **5**, showing a representative trace from the repurification of **5**. Peptide solution was injected onto a C18 semipreparative column and eluted using a linear gradient of 44-54% acetonitrile in water (constant 0.1% TFA) over 20 minutes. A small amount of impurity elutes before the desired product, but should be removed from the final product.

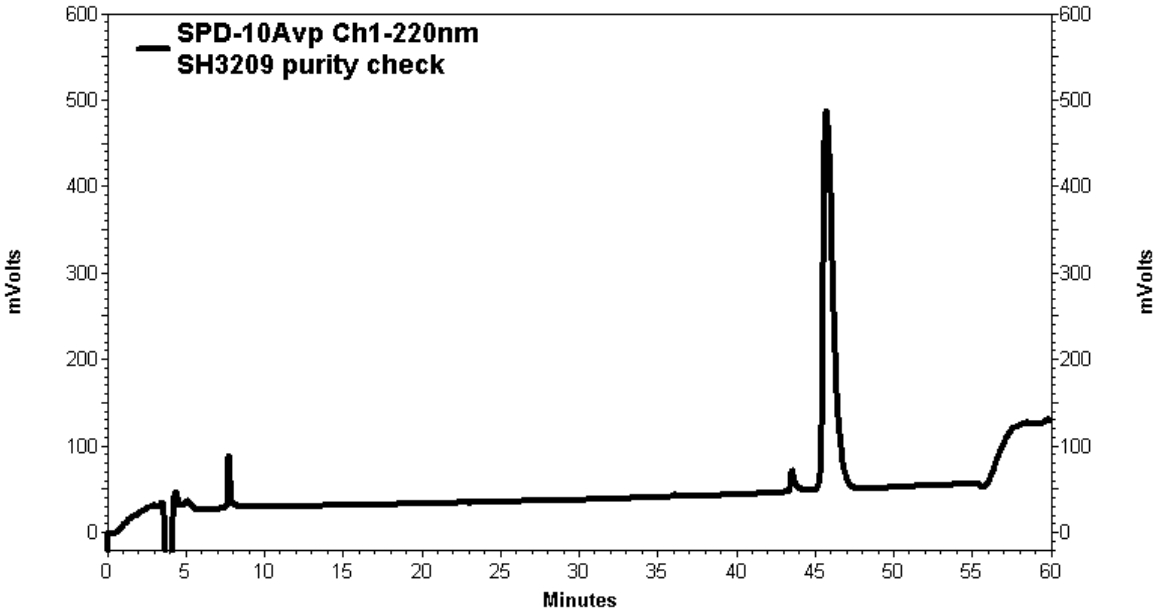

Figure S12. HPLC data for α/β-peptide **6.** Peptide solution was injected onto a C18 analytical column and eluted using a linear gradient of 10-60% acetonitrile in water (constant 0.1% TFA) over 50 minutes. Estimated purity is > 95%.

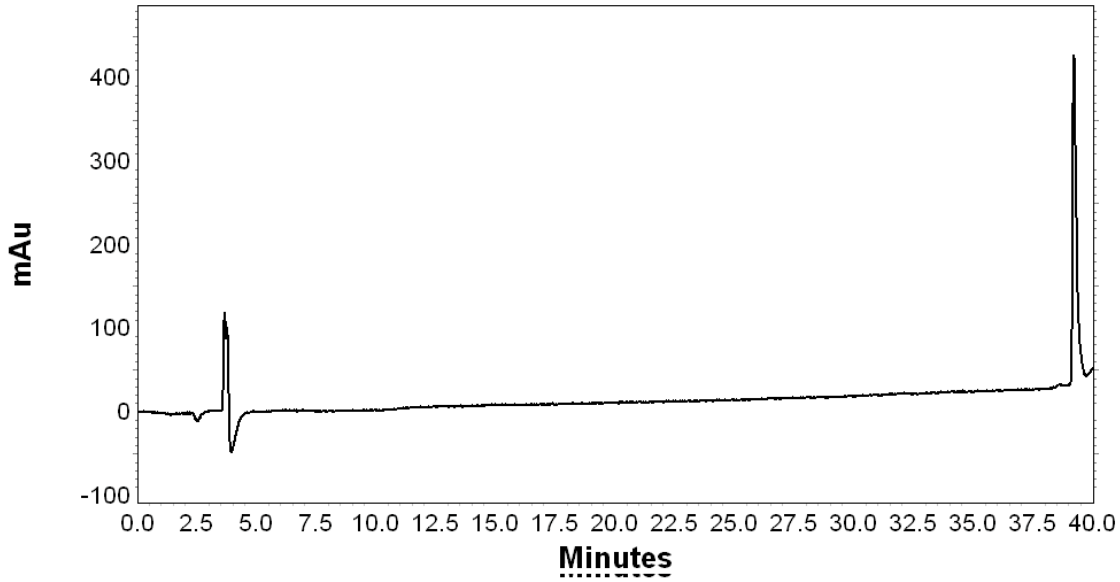

Figure S13. HPLC data for α/β-peptide **7.** Peptide solution was injected onto a C18 analytical column and eluted using a linear gradient of 30–60% acetonitrile in water (constant 0.1% TFA) over 30 minutes. Estimated purity is > 95%.

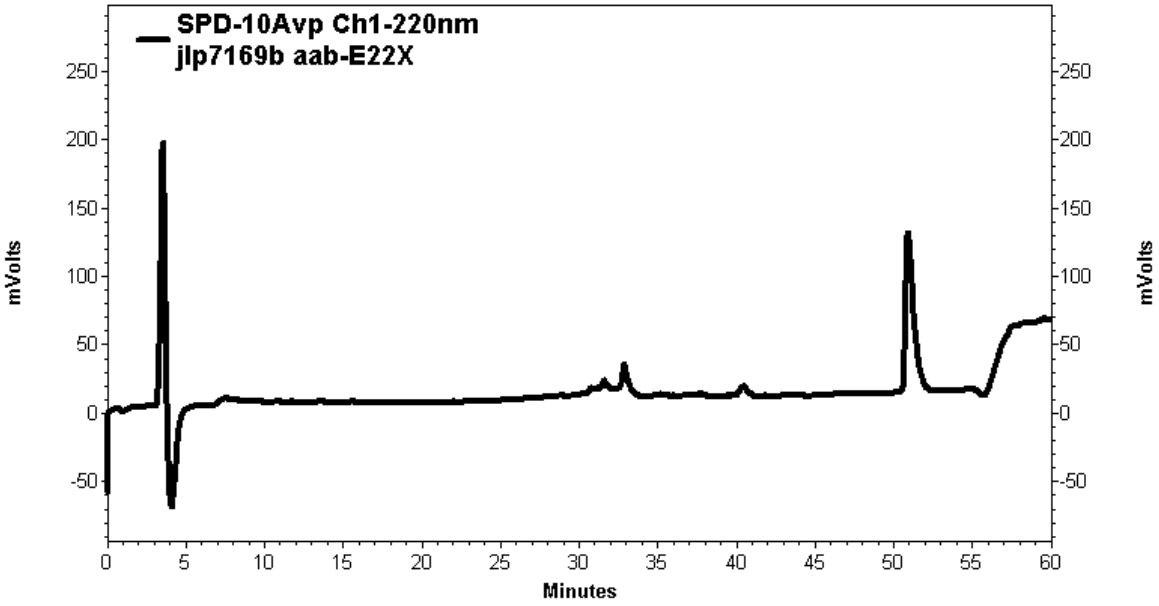

Figure S14. HPLC data for α/β-peptide **8.** Peptide solution was injected onto a C18 analytical column and eluted using a linear gradient of 10–60% acetonitrile in water (constant 0.1% TFA) over 50 minutes.

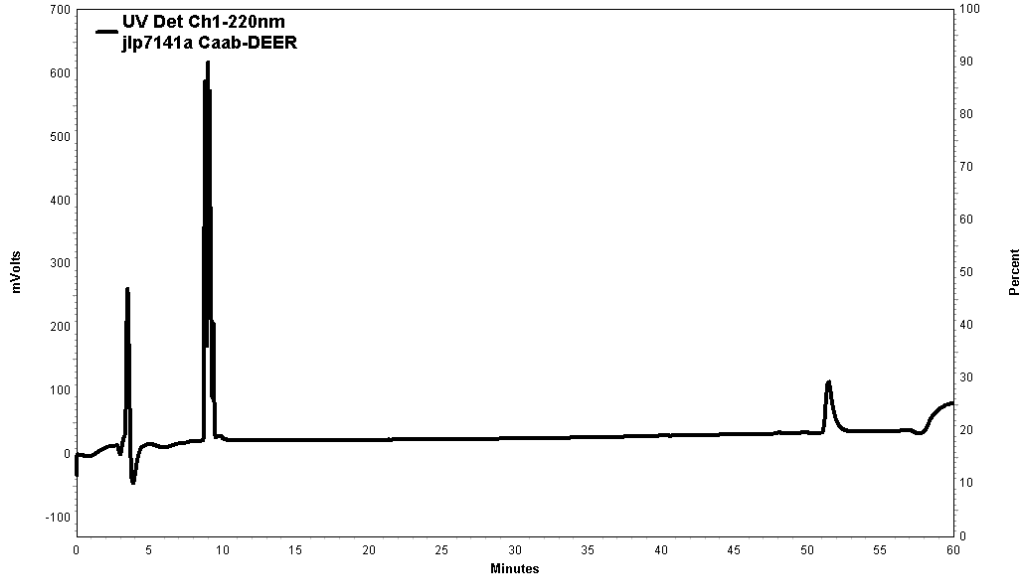

Figure S15. HPLC data for α/β-peptide **9.** Peptide solution was injected onto a C18 analytical column and eluted using a linear gradient of 10–60% acetonitrile in water (constant 0.1% TFA) over 50 minutes. The large peak near 10 minutes is probably due to a pressure fluctuation in the HPLC instrument.

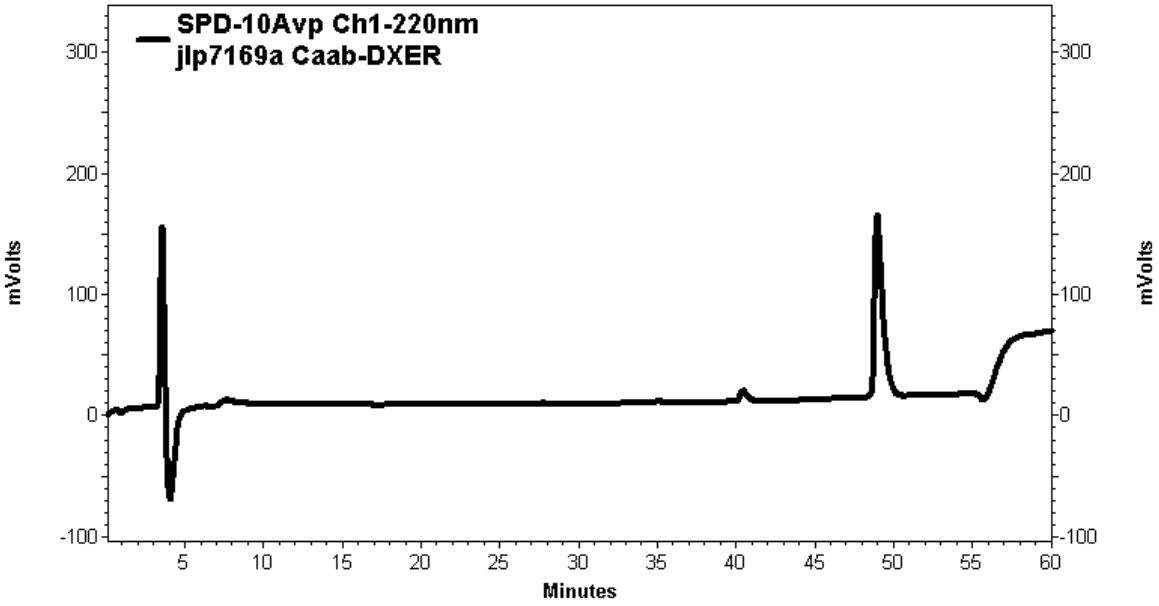

Figure S16. HPLC data for α/β-peptide **10**. Peptide solution was injected onto a C18 analytical column and eluted using a linear gradient of 10–60% acetonitrile in water (constant 0.1% TFA) over 50 minutes. Estimated purity is > 95%.

Circular Dichroism Spectroscopy

Measurements were made with an Aviv 62A DS Circular Dichroism Spectrometer, using quartz cuvettes with a 0.1 cm path length. Peptide solutions were prepared in 10 mM aqueous sodium acetate buffer, pH 4.6, and peptide concentrations were determined spectroscopically based on tyrosine absorbance at 276 nm (ε = 1450 $M^{-1}cm^{-1}$). CD spectra were obtained by monitoring molar ellipticity from 260 to 200 nm, with 5 second averaging times. Spectra were corrected for baseline molar ellipticity at 260 nm. Variable temperature CD data were obtained by monitoring molar ellipticity at 206 nm from 4 to 94 °C at 5 °C intervals or from 2 to 98 °C at 4 °C intervals, with 10 minute equilibration time between data points and 5 second averaging times.

Analytical Ultracentrifugation

Sedimentation equilibrium experiments were performed using a Beckman XLA ultracentrifuge. Peptide solutions were loaded into 1.2 cm cells, and sedimentation was monitored by absorbance at 275 nm. Sedimentation equilibria were analyzed at several speeds ranging from 12 to 60 krpm, and data were collected at 0.001 cm intervals along the length of the cell at each speed. After changing speeds, data collection was repeated every 2 hours until consecutive data sets were superimposable, signaling that the system was at equilibrium. Apparent molecular weight was determined by non-linear regression of the equilibrium radial absorbance data using the program SigmaPlot (SPSS, Inc.). Data were fit to models either for a single species, for equilibrium between monomer and *n*-mer, or for equilibria among monomer, *n*-mer and *m*-mer (equations S1–S3, respectively):

$$c_r = c_{base} + c_{ref} \exp\left[\frac{M(1-\bar{v}\rho)\omega^2}{2RT}(r^2 - r_{ref}^2)\right] \tag{S1}$$

$$\begin{aligned} c_r = c_{base} &+ c_{ref} \exp\left[\frac{M_1(1-\bar{v}\rho)\omega^2}{2RT}(r^2 - r_{ref}^2)\right] \\ &+ K_n c_{ref}^n \left[\frac{nM_1(1-\bar{v}\rho)\omega^2}{2RT}(r^2 - r_{ref}^2)\right] \end{aligned} \tag{S2}$$

$$\begin{aligned} c_r = c_{base} &+ c_{ref} \exp\left[\frac{M_1(1-\bar{v}\rho)\omega^2}{2RT}(r^2 - r_{ref}^2)\right] \\ &+ K_n c_{ref}^n \left[\frac{nM_1(1-\bar{v}\rho)\omega^2}{2RT}(r^2 - r_{ref}^2)\right] + K_m c_{ref}^m \left[\frac{mM_1(1-\bar{v}\rho)\omega^2}{2RT}(r^2 - r_{ref}^2)\right] \end{aligned} \tag{S3}$$

In equation S1, c_r is the concentration of peptide (in absorbance units) at radial position r (in cm), c_{ref} is the concentration of peptide at an arbitrary reference radial position r_{ref}, M is the apparent molecular weight of the peptide, $\bar{v}$ is the partial specific volume of the peptide (in

Table S2 MW and $\bar{v}$[a] for αααβ-peptides **3-10**

Peptide	MW ($g \cdot mol^{-1}$)	$\bar{v}$ ($cm^3 \cdot g^{-1}$)
3	4001.9	0.7673
4	4201.0	0.7671
5	4201.1	0.7705
6	4216.0	0.7616
7	4216.0	0.7616
8	4201.1	0.7705
9	4097.8	0.7534
10	4066.9	0.7586

[a]calculated according to reference 6

$cm^3 \cdot g^{-1}$), ρ is the density of the sample, ω is the radial velocity (in s^{-1}) during the measurement, R is the universal gas constant, T is the temperature (in Kelvin), and c_{base} is a correction for baseline absorbance resulting from non-sedimenting components of the sample. The variables in equation S2 have the same meaning, except c_{ref} is the concentration of the monomer (in absorbance units) at the arbitrary reference radial position, K_n is the equilibrium constant for the association between the monomer and the n-mer, n is the aggregation number for the species in equilibrium with the monomer, and M_1 is the molecular weight of the monomer. The variables in equation S3 have the same meaning except K_m is the equilibrium constant for the association between the monomer and the m-mer, and m is the aggregation number for the species in equilibrium with the monomer. The partial specific volumes for each peptide were calculated according to the method of Durchschlag and Zipper[6] and are shown in Table S2.

As a rule, equilibrium sedimentation data were fit to the single species model first; the equilibrium models were attempted if the single species fit was unsatisfactory. The quality of a particular fit was judged based on the R^2 value (closer to 1 is better), the fit standard deviation (lower is better), and the appearance of the residual plots, which show the difference between the data and the fit at each radial position (smaller and more random deviations from residual = 0 are better). If the single-species and equilibrium models were of similar quality according to these criteria, we used the simpler model to describe the peptide in Table 1 of the main text. In such cases, the single species and equilibrium model lead to the same qualitative conclusions (that a particular peptide forms a helix-bundle tetramer, for example). The best model selected for each peptide according to these criteria is highlighted with a red box in Figures S17–S24. In each case, alternative models are also presented to show how we arrived at the conclusions presented in Table 1 in the main text.

AU data for α/β-peptides **5**, **7**, **8**, and **10** (see Figures S19, S21, S22, and S24, respectively) fit well to single species models with apparent molecular weights in each case consistent with the formation of a helix-bundle tetramer, the same aggregation state observed in the crystal structures of **5**, **7**, **8**, and **10**. In contrast, AU data for α/β-peptides **3**, **4**, **6**, and **9** (see Figures S17, S18, S20, and S23, respectively) fit best to equilibrium models involving self-association of an α/β-peptide monomer to form one or two aggregated species. This result is particularly striking for α/β-peptides **6** and **9**, which form tetramers in the crystalline state.

AU data for α/β-peptide **3** (which showed diminished helicity in the CD experiments relative to other α/β-peptides) fit best to a monomer-trimer equilibrium model, in which a 100 μM solution contains 31% monomer and 69% trimer (Figure S17A). This solution behavior is interesting because **3** has nine cyclic β-residues, more than any other α/β-peptide

investigated here. We had expected **3** to be the most stable α/β-peptide because of its high cyclic β-residue content. As with α/β-peptide **6**, it is possible that having ACPC at position 13 instead of β^3Leu destabilizes the helix-bundle tetramer in preference for another aggregation state. Other ACPC substitutions present in **3**, but not present in the other α/β-peptides (at position 7 in place of β^3Asp_7 or at position 31 in place of β-homoglycine$_{31}$) may also play a role in shifting the preferred aggregation state away from the helix-bundle tetramer.

The sedimentation behavior of **4** is best described by a monomer-tetramer-pentamer equilibrium model in which a 200 μM solution of peptide contains 28% monomer, 50% tetramer, and 22% pentamer (Figure S18E). AU data for α/β-peptide **6** (which has ACPC at residue 13, and which showed diminished helicity in CD experiments relative to other α/β-peptides) fit best to a monomer-tetramer-pentamer equilibrium in which a 200 μM solution contains 10% monomer, 64% tetramer, and 26% pentamer (Figure S20E). The fact that the tetramer alone was observed in the crystal structure of **6** (see Figure 3 of the main text) could be explained by a shift of the equilibrium at higher concentration in favor of the tetramer or by the different buffer conditions involved in peptide crystallization (the crystallization buffer contained Mg^{2+}, HEPES, and PEG400, whereas the AU buffer contained sodium acetate and NaCl). Alternatively, the tetramer may be more prone to crystallization than the pentamer.

The sedimentation behavior of α/β-peptide **9** is best described by a monomer-pentamer equilibrium model, in which a 200 μM solution contains 16% monomer and 84% pentamer (Figure S23D); this result is not in agreement with the helix-bundle tetramer quaternary structure observed in the crystal structure of **9**. As for α/β-peptide **6**, our observation of a

helix-bundle tetramer in the crystal structure of **9** could indicate a shift of the self-association equilibrium to prefer the tetramer at the high concentrations required for crystallization.

It is interesting to note the contrast between AU and variable temperature CD data for α/β-peptides **4** and **9**. Though AU results indicate that each of these α/β-peptides is involved in an equilibrating mixture of aggregated species at room temperature, the $[\theta]_{206}$ for each peptide shows little variation with increasing temperature up to ~60 °C. This discrepancy between AU and variable temperature CD results may reflect uncertainties in the AU-derived equilibrium constants, which were obtained by fitting the AU data from a single experiment on a given α/β-peptide at a single peptide concentration. It is possible that global fits of additional AU experiments (performed at multiple peptide concentrations) could provide values for equilibrium constants that would be consistent with the CD data. Alternatively, it is possible that the self-association behavior of **4** and **9** is more complicated than any of the simple models presented here and perhaps involves other aggregated species.

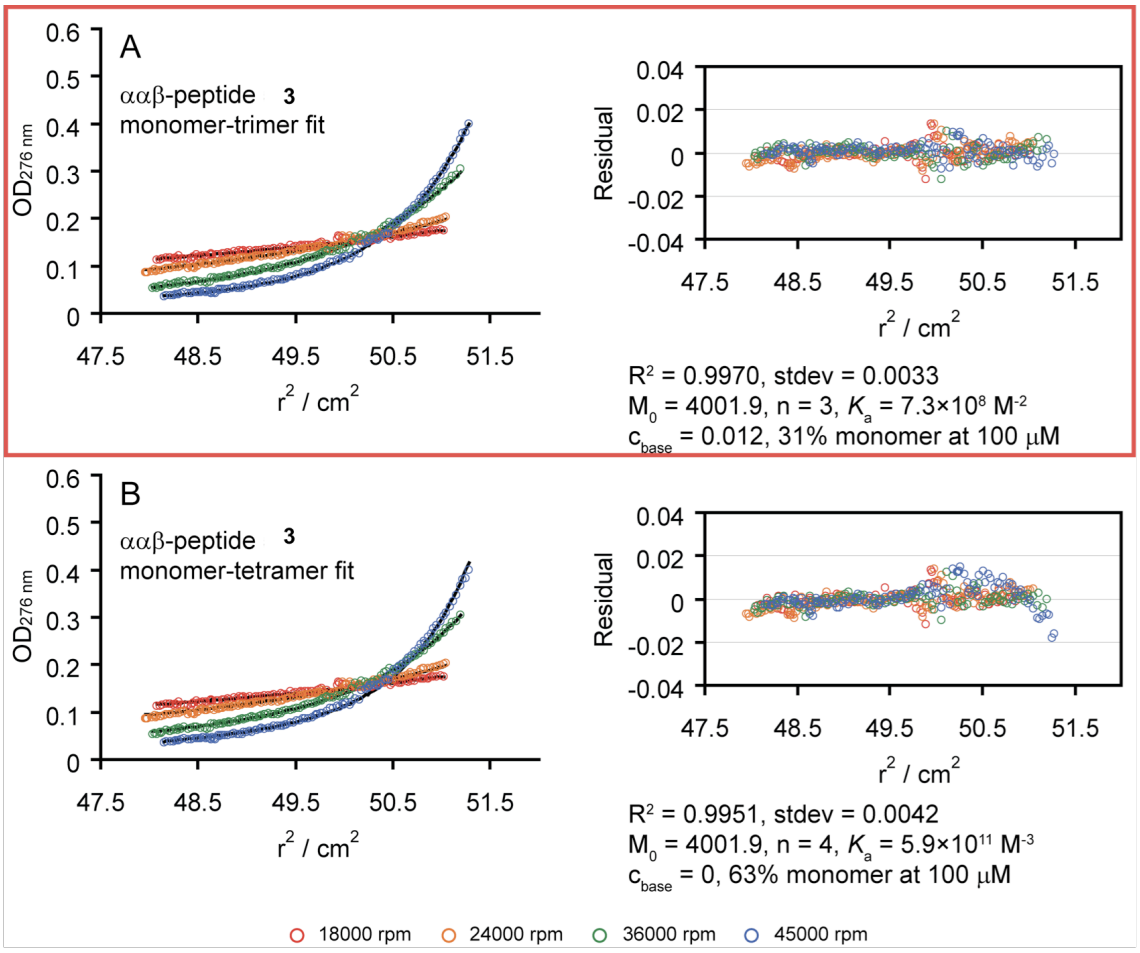

Figure S17. AU data for 100 μM α/β-peptide **3** in 10 mM sodium acetate (pH 4.6) at 25 °C, and at rotor speeds of 18000 (red circles), 24000 (orange circles), 36000 (green circles), and 45000 rpm (blue circles). Black lines represent fits of the data to (A) monomer-trimer equilibrium mode, and (B) a monomer-tetramer equilibrium model. The ability of either model to describe the sedimentation behavior of **3** was assessed based on the R^2 value (closer to 1 is better), the fit standard deviation (lower is better), and the residual plots to the right, which show the difference between observed and fitted values at each speed and concentration (smaller and more random deviations from residual = 0 are better). Based on these criteria, the sedimentation behavior of α/β-peptide **3** is best described by the monomer-trimer model shown in (A) and outlined with a red box. The equilibrium constant for this monomer-trimer model suggests that a 100 μM solution of **3** would contain 31% monomer and 69% trimer.

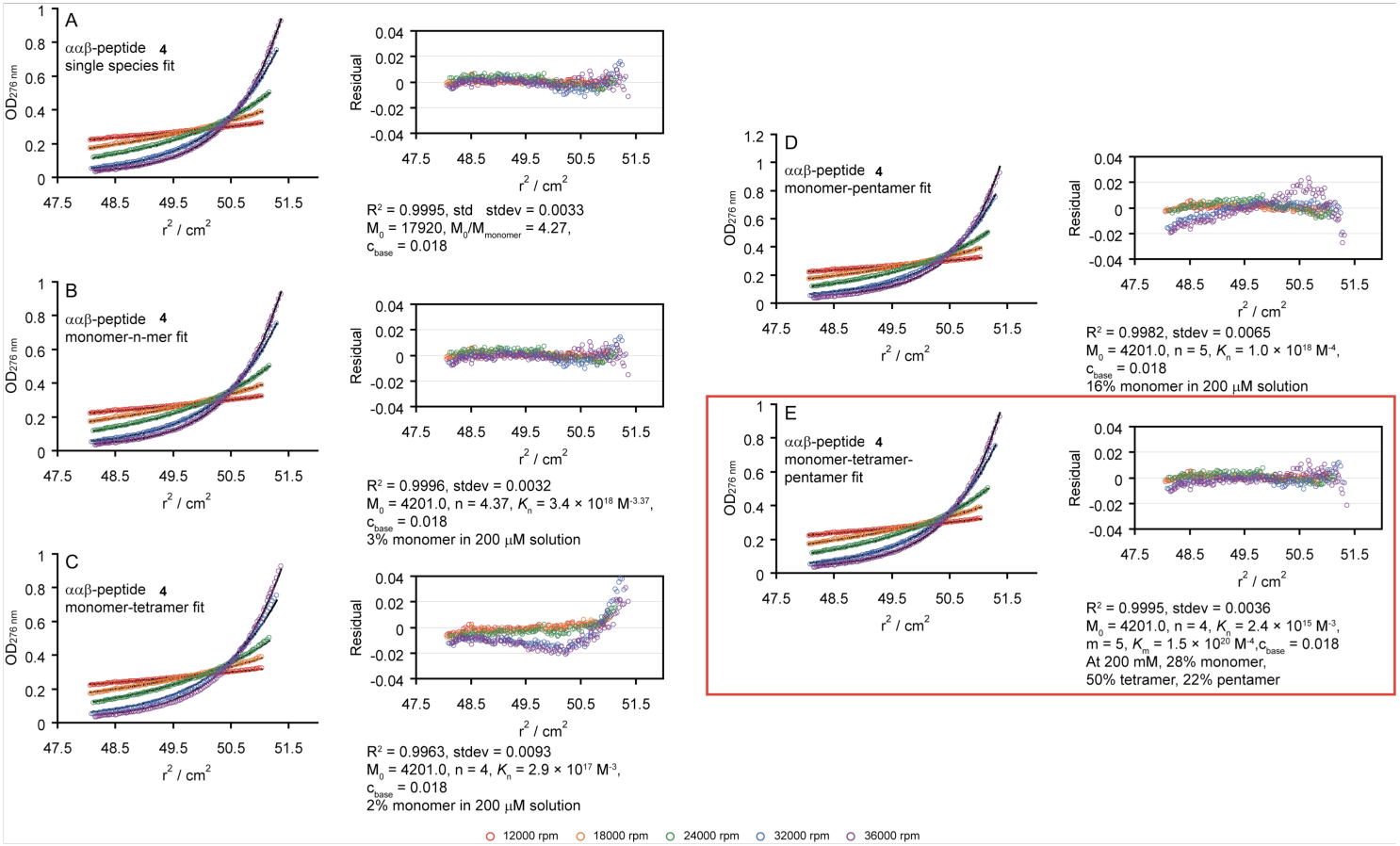

Figure S18. AU data for 200 μM α/β-peptide **4** in 10 mM sodium acetate (pH 4.6) and 150 mM NaCl at 25 °C, and at rotor speeds of 12000 (red circles), 18000 (orange circles), 24000 rpm (green circles), 32000 (blue circles) and 36000 rpm (purple circles). Black lines represent fits of the data to (A) a single species model, (B) a monomer-n-mer equilibrium model, (C) a monomer-tetramer equilibrium fit, (D) a monomer-pentamer fit, and (E) a monomer-tetramer-pentamer equilibrium fit. The ability of either model to describe the sedimentation behavior of **4** was assessed based on the R^2 value (closer to 1 is better), the fit standard deviation (lower is better), and the residual plots to the right of each graph, which show the difference between observed and fitted values at each speed and concentration (smaller and more random deviations from residual = 0 are better). Based on these criteria, the sedimentation behavior of α/β-peptide **4** is best described by the equilibrium model shown in (E) and outlined with a red box. The equilibrium constants for this fit suggest that a 200 μM solution of **4** would contain 28% monomer, 50% tetramer, and 22% pentamer.

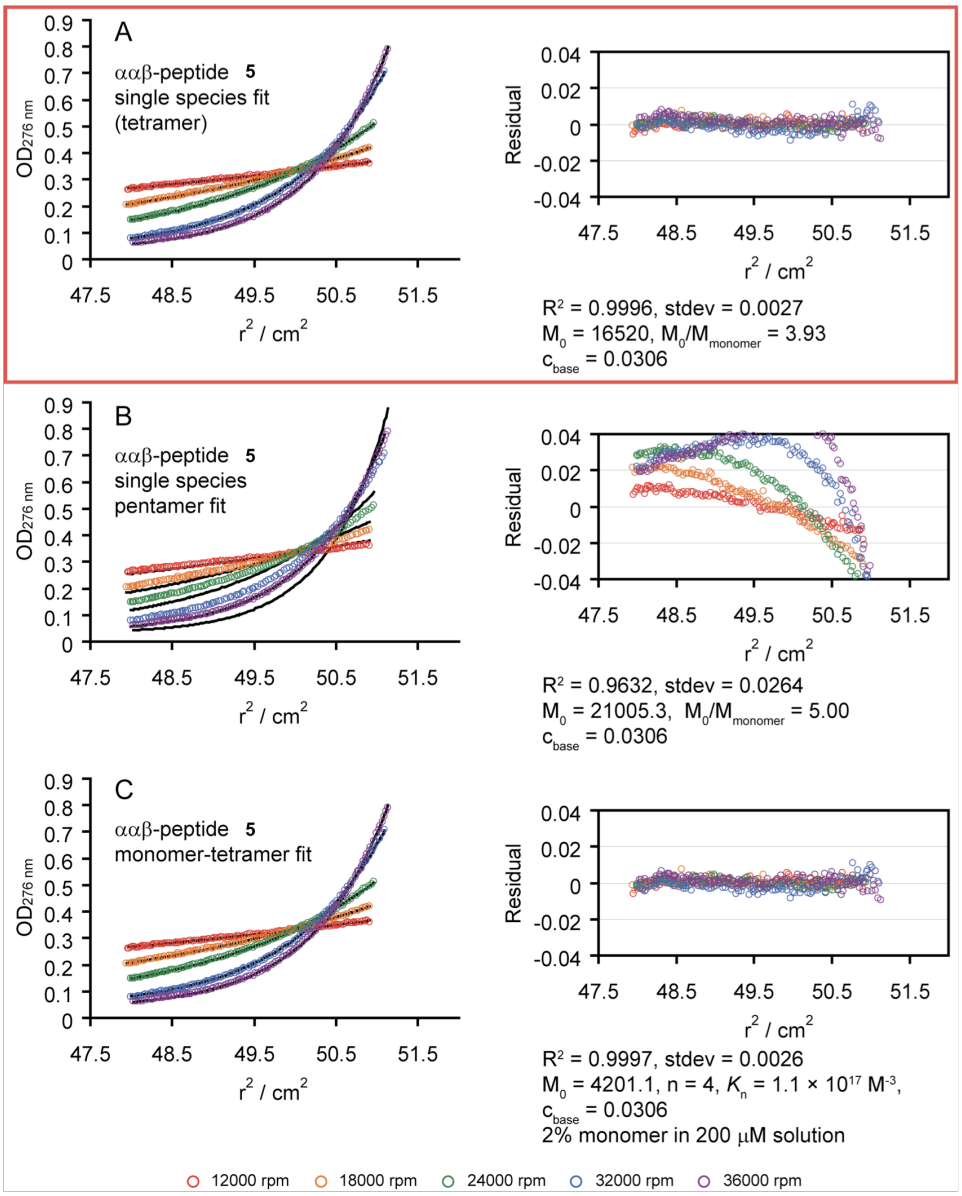

Figure S19. AU data for 200 μM α/β-peptide **5** in 10 mM sodium acetate (pH 4.6) and 150 mM NaCl at 25 °C, and at rotor speeds of 12000 (red circles), 18000 (orange circles), 24000 (green circles), 32000 (blue circles), and 36000 rpm (purple circles). Black lines represent fits of the data to (A) a single species model, (B) a single species pentamer model, and (C) a monomer-tetramer equilibrium model. The ability of either model to describe the sedimentation behavior of **5** was assessed based on the R^2 value (closer to 1 is better), the fit standard deviation (lower is better), and the residual plots to the right, which show the difference between observed and fitted values at each speed and concentration (smaller and more random deviations from residual = 0 are better). Based on these criteria, the sedimentation behavior of α/β-peptide **5** is best described either by the single species model shown in (A) and outlined with a red box, or by the monomer-tetramer model shown in (C). The apparent molecular weight of **5** obtained from the single species fit (16520 g·mol^{-1}) compares favorably with the expected molecular weight of a tetramer (16804.2 g·mol^{-1}, a 2% difference). The high magnitude of the equilibrium constant in (C) indicates that a 200 μM solution of peptide would contain 2% monomer, and 98% tetramer, suggesting that the description of α/β-peptide **5** as a single species tetramer is sufficient.

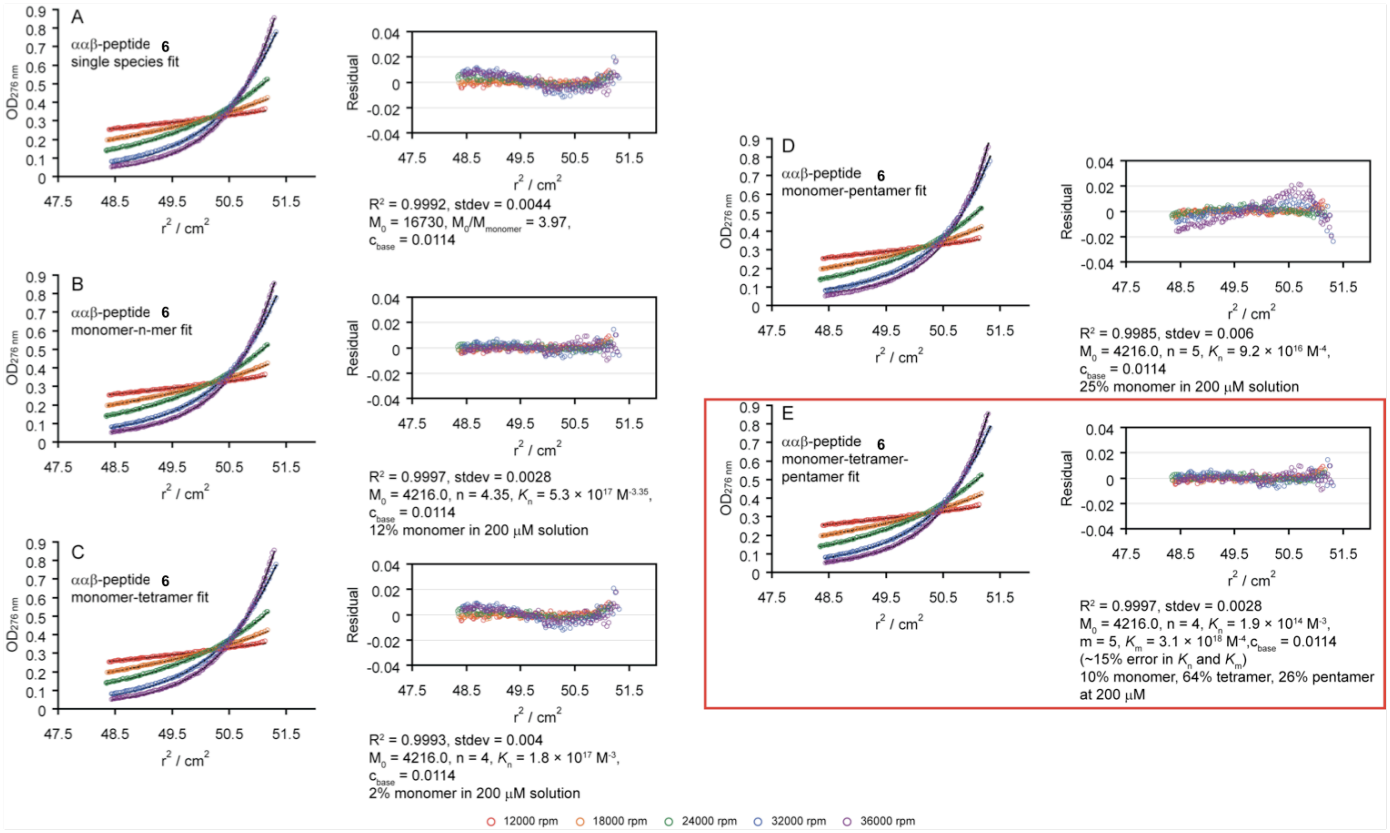

Figure S20. AU data for 200 μM α/β-peptide **6** in 10 mM sodium acetate (pH 4.6) and 150 mM NaCl at 25 °C, and at rotor speeds of 12000 (red circles), 18000 (orange circles), 24000 rpm (green circles), 32000 (blue circles) and 36000 rpm (purple circles). Black lines represent fits of the data to (A) a single species model, (B) a monomer-n-mer equilibrium model, (C) a monomer-tetramer equilibrium fit, (D) a monomer-pentamer fit, and (E) a monomer-tetramer-pentamer equilibrium fit. The ability of either model to describe the sedimentation behavior of **6** was assessed based on the R^2 value (closer to 1 is better), the fit standard deviation (lower is better), and the residual plots to the right of each graph, which show the difference between observed and fitted values at each speed and concentration (smaller and more random deviations from residual = 0 are better). Based on these criteria, the sedimentation behavior of α/β-peptide **6** is best described by the equilibrium model shown in (E) and outlined with a red box. The equilibrium constants obtained from this fit suggest that a 200 μM solution of **6** would contain 10% monomer, 64% tetramer, and 26% pentamer. However, these equilibrium constants have a high level of uncertainty (~15%), which may suggest that the behavior of **6** is more complicated than the monomer-tetramer-pentamer equilibrium model described here.

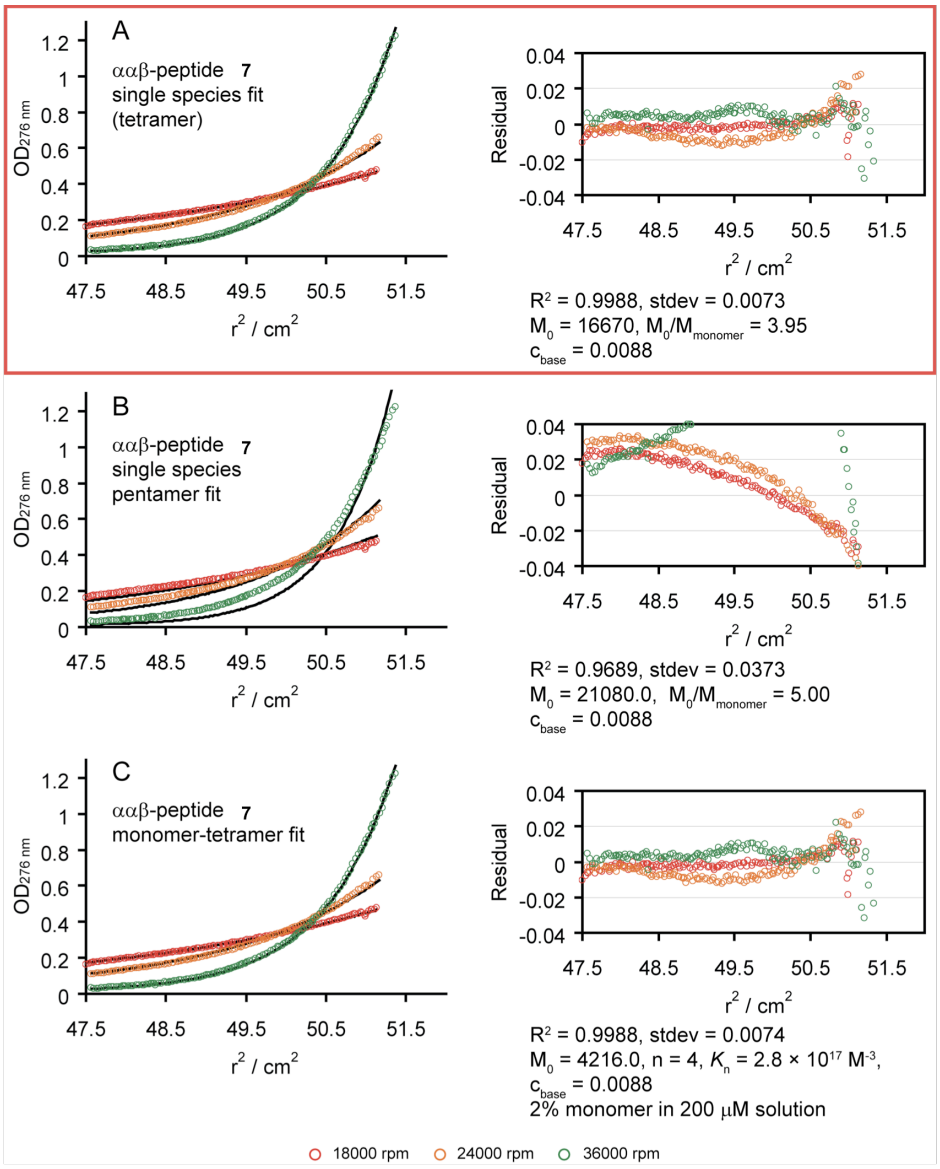

Figure S21. AU data for 200 μM α/β-peptide **7** in 10 mM sodium acetate (pH 4.6) and 150 mM NaCl at 25 °C, and at rotor speeds of 18000 (red circles), 24000 (orange circles), 36000 rpm (green circles). Black lines represent fits of the data to (A) a single species model, (B) a single species pentamer model, and (C) a monomer-tetramer equilibrium model. The ability of each model to describe the sedimentation behavior of **7** was assessed based on the R^2 value (closer to 1 is better), the fit standard deviation (lower is better), and the residual plots to the right, which show the difference between observed and fitted values at each speed and concentration (smaller and more random deviations from residual = 0 are better). Based on these criteria, the sedimentation behavior of α/β-peptide **7** is best described either by the single species model shown in (A) and outlined with a red box, or by the monomer-tetramer model shown in (C). The apparent molecular weight of **7** obtained from the single species fit (16670 g·mol^{-1}) compares favorably with the expected molecular weight of a tetramer (16864.0 g·mol^{-1}, a 1% difference). The high magnitude of the equilibrium constant in (C) indicates that a 200 μM solution of peptide would contain 2% monomer, and 98% tetramer, suggesting that the description of α/β-peptide **7** as a single species tetramer is sufficient. However, the strange shape the residuals in (A) could indicate that the behavior of **7** is more complicated. More AU experiments at more than one concentration could potentially provide additional insight.

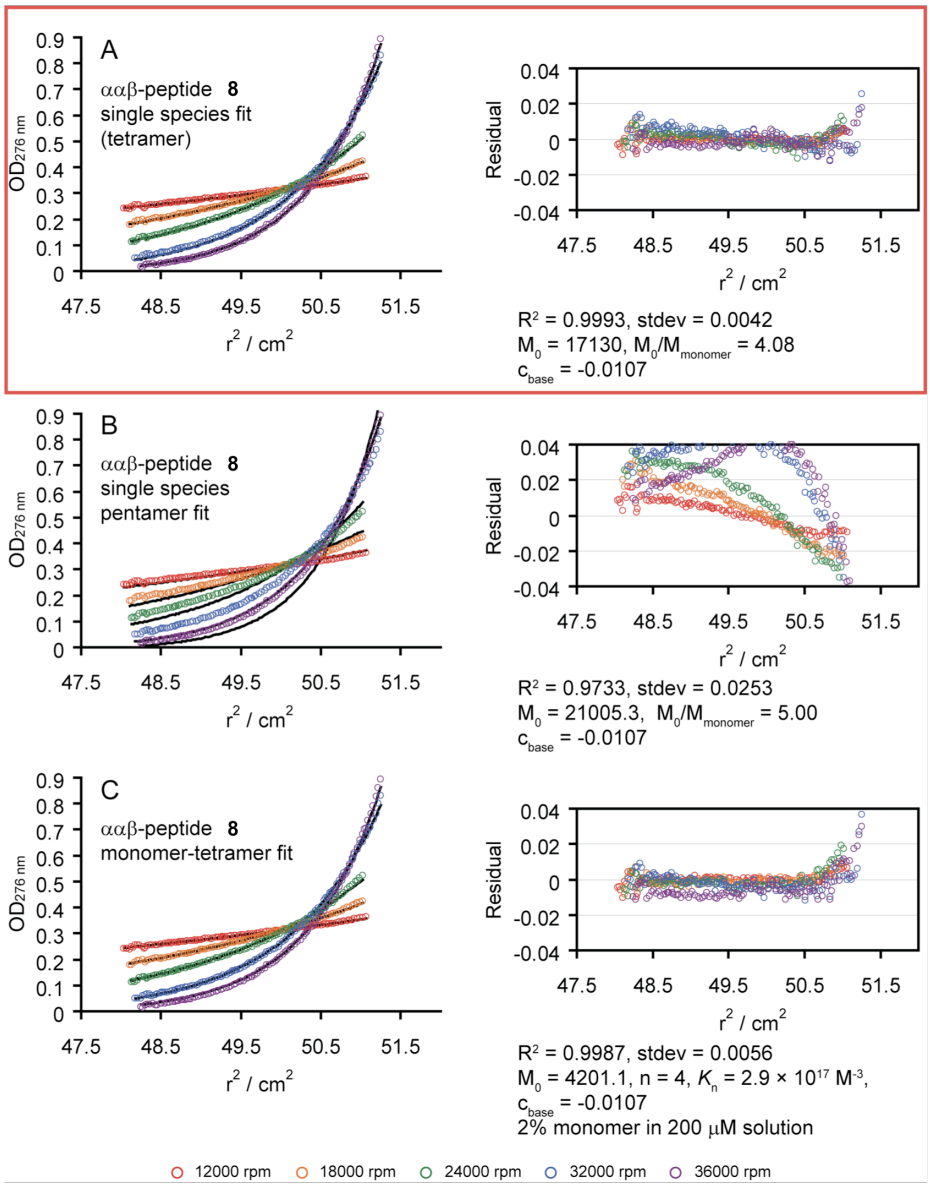

Figure S22 AU data for 200 μM α/β-peptide **8** in 10 mM sodium acetate (pH 4.6) and 150 mM NaCl at 25 °C, and at rotor speeds of 12000 (red circles), 18000 (orange circles), 24000 (green circles), 32000 (blue circles), and 36000 rpm (purple circles). Black lines represent fits of the data to (A) a single species model, (B) a single species pentamer model, and (C) a monomer-tetramer equilibrium model. The negative baseline value used for each fit (c_{base}=-0.107) was obtained from the absorbance in the "depleted region" near the meniscus in the 60000 rpm data set. The ability of either model to describe the sedimentation behavior of **8** was assessed based on the R^2 value (closer to 1 is better), the fit standard deviation (lower is better), and the residual plots to the right, which show the difference between observed and fitted values at each speed and concentration (smaller and more random deviations from residual = 0 are better). Based on these criteria, the sedimentation behavior of α/β-peptide **8** is best described by the single species model shown in (A) and outlined with a red box. The apparent molecular weight of **8** obtained from the single species fit (17130 g·mol^{-1}) compares favorably with the expected molecular weight of a tetramer (16804.2 g·mol^{-1}, a 2% difference).

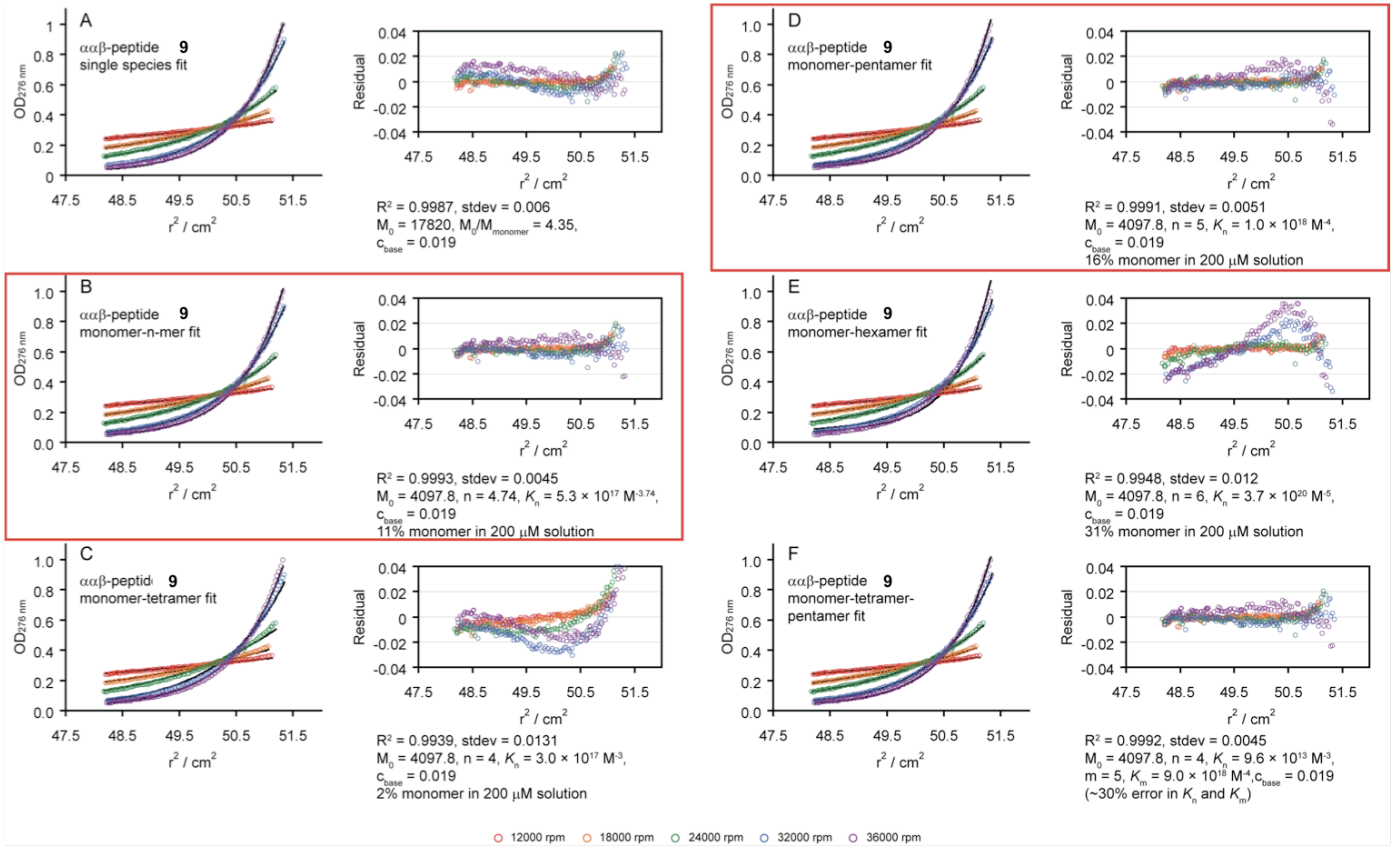

Figure S23. AU data for 200 μM α/β-peptide **9** in 10 mM sodium acetate (pH 4.6) and 150 mM NaCl at 25 °C, and at rotor speeds of 12000 (red circles), 18000 (orange circles), 24000 rpm (green circles), 32000 (blue circles) and 36000 rpm (purple circles). Black lines represent fits of the data to (A) a single species model, (B) a monomer-n-mer equilibrium model, (C) a monomer-tetramer model, (D) a monomer-pentamer model, (E) a monomer-hexamer model, and (F) a monomer-tetramer-pentamer model. The ability of each model to describe the sedimentation behavior of **9** was assessed based on the R^2 value (closer to 1 is better), the fit standard deviation (lower is better), and the residual plots to the right of each graph, which show the difference between observed and fitted values at each speed and concentration (smaller and more random deviations from residual = 0 are better). Based on these criteria, the sedimentation behavior of α/β-peptide **9** is best similarly well by the equilibrium models shown in (B) and (D) and outlined with red boxes, suggesting that a 200 μM solution of **9** contains ~11-16% monomer and 84-89% pentamer. The residuals in (B) and (D) are not as randomly distributed about zero as they could be, and though (B) and (D) represent the best of the models presented here, it is possible that the self-association behavior of **9** could be more complicated than a monomer-penatmer equilibrium

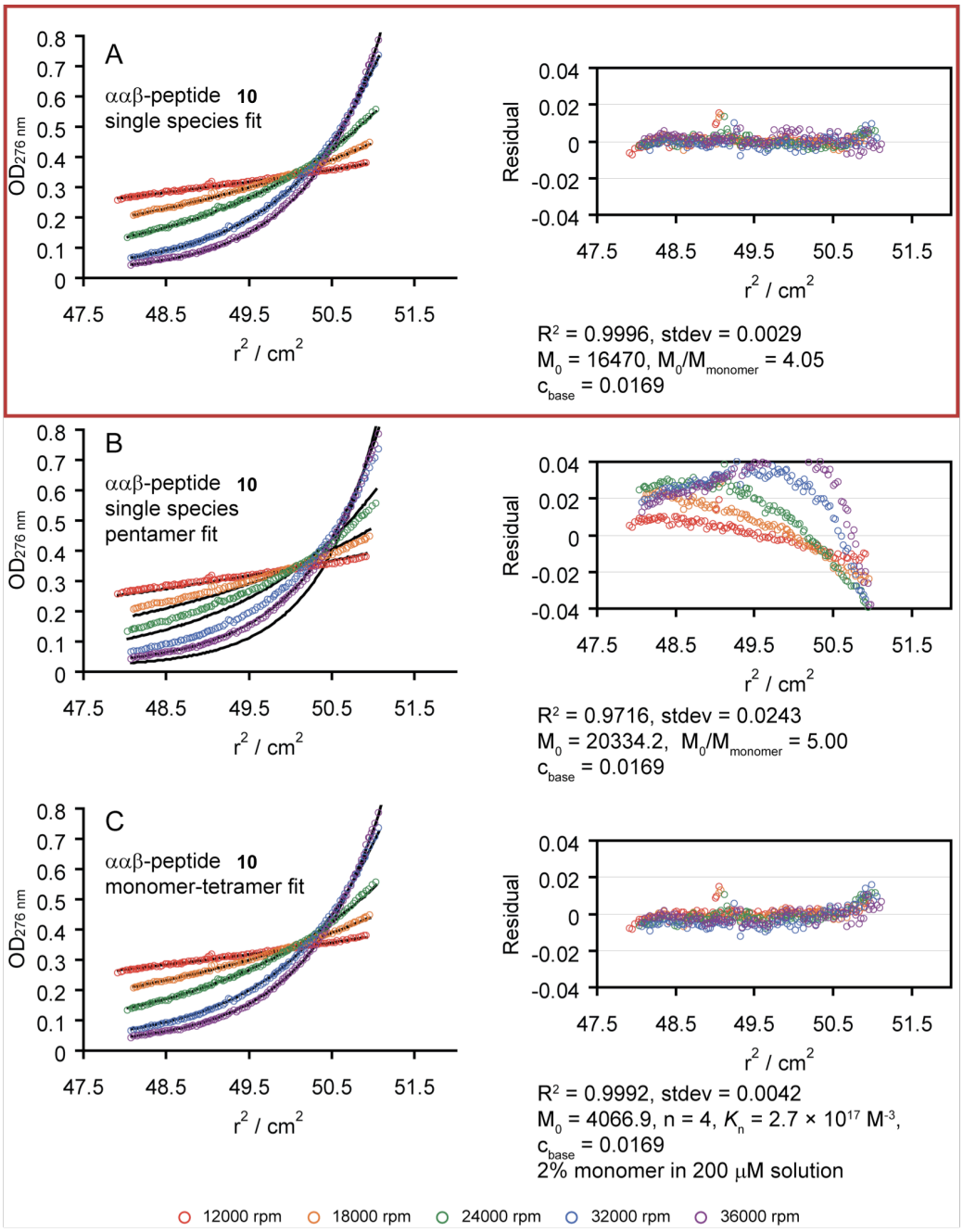

Figure S24. AU data for 200 μM α/β-peptide **10** in 10 mM sodium acetate (pH 4.6) and 150 mM NaCl at 25 °C, and at rotor speeds of 12000 (red circles), 18000 (orange circles), 24000 (green circles), 32000 (blue circles), and 36000 rpm (purple circles). Black lines represent fits of the data to (A) a single species model, (B) a single species pentamer model, and (C) a monomer-tetramer equilibrium model. The ability of either model to describe the sedimentation behavior of **10** was assessed based on the R^2 value (closer to 1 is better), the fit standard deviation (lower is better), and the residual plots to the right, which show the difference between observed and fitted values at each speed and concentration (smaller and more random deviations from residual = 0 are better). Based on these criteria, the sedimentation behavior of α/β-peptide **10** is best described by the single species model shown in (A) and outlined with a red box. The apparent molecular weight of **10** obtained from the single species fit (16470 g·mol^{-1}) compares favorably with the expected molecular weight of a tetramer (16267.4 g·mol^{-1}, a 1% difference).

X-ray Crystallography

Peptide Crystallization

α/β-peptides **5**–**10** were crystallized by the hanging drop vapor diffusion method. Peptide stock solutions were ~10 mg/mL in water and mixed 1:1 with the crystallization buffers indicated prior to equilibration. α/β-Peptide **5** was crystallized from 0.05 M CsCl, 0.1 M MES pH 6.5, 30% v/v Jeffamine M-600, and the crystal was frozen directly from the parent buffer. α/β-Peptide **6** was crystallized from 0.1 M $MgCl_2 \cdot 6H_2O$, 0.1 M HEPES-Na pH 7.5, 30% v/v PEG 400, and the crystal was frozen directly from the parent buffer. α/β-Peptide **7** was crystallized from 1.6 M $(NH_4)_2SO_4$, 0.1 M MES pH 6.5, 10% v/v dioxane, and the crystal was frozen after cryoprotection in the above buffer supplemented with 25% v/v glycerol. α/β-Peptide **8** was crystallized from 0.1 M Tris pH 8.5, 0.7 M diammonium tartrate, and the crystal was frozen after cryoprotection in 0.1 M Tris pH 8.5, 1 M diammonium tartrate, 30% v/v glycerol. α/β-Peptide **9** was crystallized from 0.1 M NaOAc pH 4.6, 0.35 M magnesium formate, and the crystal was frozen after cryoprotection in 0.19 M NaOAc pH 4.6, 0.26 M magnesium formate, 25% v/v glycerol. α/β-Peptide **10** was crystallized from 0.3 M NaOAc pH 4.6, 0.25 M magnesium formate, and the crystal was frozen after cryoprotection in 0.19 M NaOAc pH 4.6, 0.26 M magnesium formate, 25% v/v glycerol. Crystals were frozen in liquid nitrogen prior to data collection.

Data Collection

Diffraction data were collected on a Bruker X8 Proteum Diffractometer using Cu *Kα* radiation. Data were indexed, integrated, and scaled with the Bruker Protem2 software package.

Structure Determination

Structure solution was carried out using the CCP4 software suite.[7] Molecular replacement was carried out with Phaser.[8] The refined structure of **1** was used as a search model to solve the structures of **5**, **6**, **7**, and **8**. The refined structure of **7** was used to solve the structures of **9** and **10**. The same R_{free} sets (from the data set used to solve **1**) were used during the refinement of **5**, **6**, **7**, **8**, **9**, and **10** in order to avoid contamination of the test sets among the closely related structures. Refinement was accomplished by a combination of Refmac[9] for automated refinement, Coot[10] for manual model building, and ARP/wARP[11] for map improvement by free atom density modification and water building. A Refmac library containing geometric restraints for the β-amino acid residues as well as the α→β and β→α amide linkages was included in the refinement (see Table S3).

Table S3. Crystal data collection and refinement statistics.*

	5	6	7	8	9	10
PDB code	3HET	3HEU	3HEV	3HEW	3HEX	3HEY
Data Collection						
Unit cell dimensions (Å, °)	$a = b = 39.1$, $c = 93.3$ $\alpha = \beta = \gamma = 90$	$a = b = 37.8$, $c = 47.0$ $\alpha = \beta = \gamma = 90$	$a = b = 38.9$, $c = 46.4$ $\alpha = \beta = \gamma = 90$	$a = b = 38.5$, $c = 46.8$ $\alpha = \beta = \gamma = 90$	$a = b = 38.1$, $c = 46.1$ $\alpha = \beta = \gamma = 90$	$a = b = 38.6$, $c = 46.1$ $\alpha = \beta = \gamma = 90$
Space group	P 4 2_1 2	P 4 2_1 2	P 4 2_1 2	P 4 2_1 2	P 4 2_1 2	P 4 2_1 2
Resolution (Å)	39.11–2.10 (2.19-2.1)	47.1–2.0 (2.1-2.0)	46.4–2.0 (2.1-2.0)	46.8–2.0 (2.1–2.0)	38.12–2.8 (2.89-2.8)	46.07–2.0 (2.1-2.0)
Total observations	33,713	25,445	12,072	47,923	5,371	24,122
Unique observations	4,651	2,446	2,674	2,646	995	2,612
Redundancy	7.2 (3.0)	10.4 (4.0)	4.5 (2.9)	18.1 (6.0)	5.4 (5.8)	9.2 (3.2)
Completeness (%)	99.2 (95.0)	99.8 (98.7)	99.2 (98.3)	99.9 (100)	99.4 (100)	99.3 (94.8)
I/σ	19.6 (4.9)	21.5 (3.4)	14.6 (2.5)	35.9 (7.0)	9.1 (4.5)	29.5 (5.2)
R_{sym} (%)†	6.1 (18.9)	7.2 (34.2)	4.9 (32.1)	4.9 (21.0)	12.1 (35.3)	4.6 (20.3)
Refinement						
Resolution (Å)	25.0–2.1	25.0–2.0	25.0–2.0	25.0–2.0	25.0–2.8	25.0–2.0
R (%)	19.1	20.3	23.8	21.5	27.3	20.6
R_{free} (%)‡	23.4	24.5	28.5	25.5	29.8	25.6
Avg. B factor (Å^2)	11.6	13	19.9	16.8	25.7	14.6
RMSD						
Bonds (Å)	0.014	0.012	0.015	0.015	0.014	0.013
Angles (°)	2.0	2.0	2.1	2.2	2.0	2.1

*Values in parentheses are for data from the highest resolution shell in each data set. †$R_{sym} = \sum_n | I_n - \langle I \rangle | / \sum_n I_n$ where I_n is the intensity of an independent observation of reflection n and $\langle I \rangle$ is the average of multiply recorded and symmetry related observations of reflection n.

‡Free R reflections (~5% of total) were held aside throughout refinement

Analysis of Backbone Dihedral Angles in α/β-Peptides 5-10

Table S4. Average backbone dihedral angles for α- and β-residues in α/β-peptides **1**, **2**, **5-10**.[a]

	ideal α-helix[b]	**1**	**2**	**5**	**6**	**7**	**8**	**9**	**10**	**overall**
α-Residues										
φ (°)	-57	-67 ± 4	-65 ± 4	-65 ± 5	-65 ± 4	-68 ± 4	-66 ± 5	-64 ± 7	-66 ± 4	-66 ± 2
ψ (°)	-47	-45 ± 8	-45 ± 4	-45 ± 4	-45 ± 3	-43 ± 3	-45 ± 4	-45 ± 6	-46 ± 3	-45 ± 1
β^3-Residues										
φ (°)		-111 ± 6	-109 ± 12	-112 ± 6	-114 ± 3	-114 ± 6	-111 ± 5	-119 ± 9	-111 ± 8	-113 ± 2
θ (°)		81 ± 3	83 ± 5	82 ± 3	80 ± 3	80 ± 3	81 ± 3	83 ± 4	84 ± 4	82 ± 1
ψ (°)		-109 ± 4	-108 ± 2	-107 ± 4	-107 ± 4	-105 ± 6	-107 ± 4	-106 ± 10	-108 ± 3	-107 ± 2
Cyclic β-Residues[c]										
φ (°)			-119 ± 10	-113	-108	-109	-112	-119 ± 14	-116 ± 5	-116 ± 4
θ (°)			91 ± 13	85	82	84	81	87 ± 7	86 ± 3	87 ± 4
ψ (°)			-102 ± 6	-102	-99	-111	-109	-113 ± 12	-107 ± 10	-106 ± 2

[a]Average backbone dihedral angles (and 95% confidence intervals) in residues 2-29 from a single chain in the crystal structures of **1** (PDB 3C3G), **2** (PDB 3C3H), **5** (PDB 3HET), **6** (PDB 3HEU), **7** (PDB 3HEV), **8** (PDB 3HEW), **9** (PDB 3HEX), and **10** (PDB 3HEY).
[b]See references 12-15.
[c]The tabulated values for φ, θ, and ψ for α/β-peptides **5-8** are for single cyclic β-residues and do not represent averages.

Analysis of Structural Differences Between α/β-Peptide 6 and α/β-Peptides 1, 5, 7-10

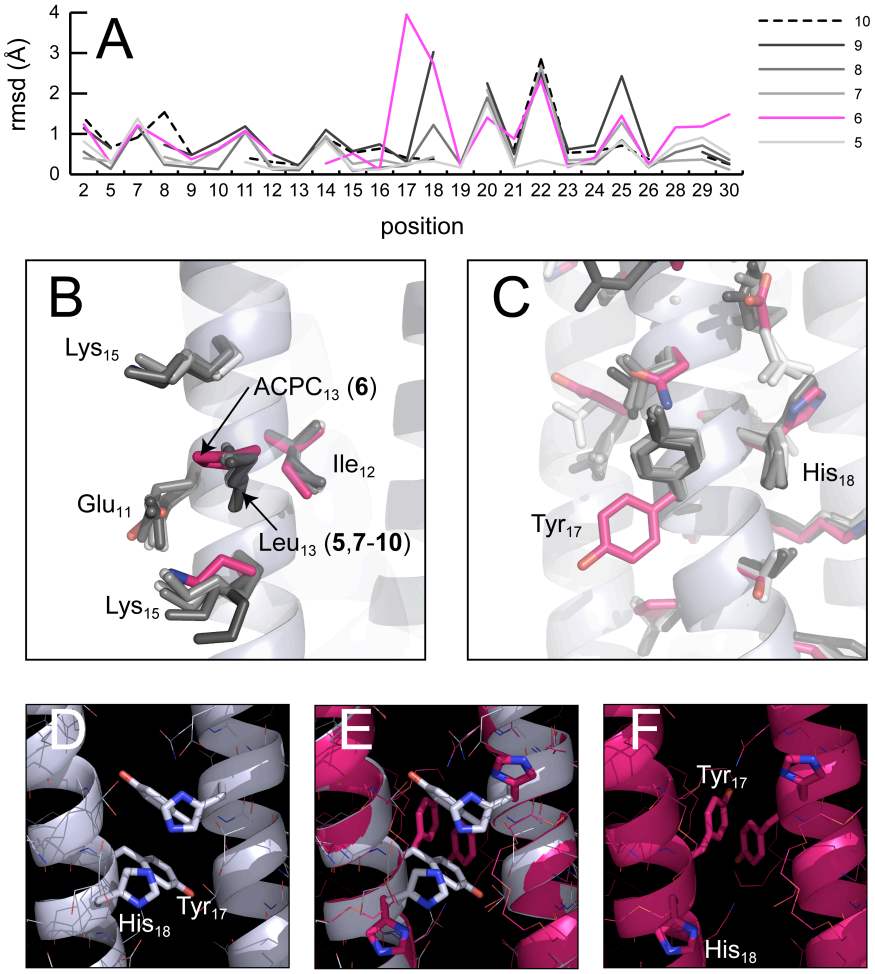

Figure S25. (A) Root-mean-square deviation between individual residues of α/β-peptides **5**-**10** (PDB 3HET, 3HEU, 3HEV, 3HEW, 3HEY, and 3HEX, respectively) and corresponding individual residues of α/β-peptide **1** (PDB 3C3G). The deviation between **6** and **1** is abnormally high at Tyr_{17} relative to the deviations between **5**, **7**-**10** and **1** at the same position. The deviation between **6** and **1** is also high at His_{18} relative to the deviations between **5**, **7**, **8**, and **10** at the same position (the deviation between **9** and **1** is also high at this position). (B) Overlay of side-chains from positions 8, 11, 12, 13 and 15, from α/β-peptides **1**, **5**-**10** superimposed on the ribbon diagram of the helix-bundle formed by α/β-peptide **1**. Side-chains at each of these positions overlay quite well and do not provide structural evidence for a repulsive steric interaction between $ACPC_{13}$ in **6** with nearby backbone or side-chain atoms. (C) Tyr_{17} and His_{18} side-chains adopt significantly different conformations in **6** than they do in **1**, **5**-**10** (with the exception of His_{18} in **9**, which shares a similar conformation to His_{18} in **6**). (D) Inter-helix-bundle crystal contacts between Tyr_{17} side chains and between His_{18} side-chains in **1**. (E) Overlay of inter-helix-bundle crystal contacts in **6** and **1**. (F) Inter-helix-bundle crystal contacts between Tyr_{17} side chains in **6**.

In the main text, we noted that α/β-peptide **6** contains a cyclic residue at just one position ($ACPC_{13}$), but that this cyclic residue causes a substantial destabilization of helix-bundle quaternary structure in **6** relative to **1**, which contains no cyclic residues. We hypothesized that the difference in quaternary structural stability between **1** and **6** is a result of steric repulsions experienced by the non-backbone atoms of $ACPC_{13}$ in the folded/assembled state that overwhelm the conformational benefits of limiting backbone flexibility. Repulsive interactions involving $ACPC_{13}$ in **6** are not immediately apparent upon comparing the crystal structures of **6** and **1** (Figure S25B), though such interactions could be important, especially if the *solution* and *crystal* structures of **6** differ significantly. There are some structural differences between **6** and **1** at other locations in **6**: the conformations adopted by Tyr_{17} and His_{18} in **6** differ significantly from those in **1** (Figure S25A,C), and it is possible that these structural differences are related to the diminished stability of **6** relative to **1**. However, Tyr_{17} and His_{18} are involved in inter-helix bundle lattice packing contacts in both **6** and **1** (Figure S25D-F) and these differences may reflect the influence of lattice packing more than the effect of the $\beta^3hLeu_{13} \rightarrow ACPC_{13}$ mutation in **6**. It is possible that destabilizing interactions involving $ACPC_{13}$ in the solution structure of **6** are relieved upon crystallization of **6** by rearrangement of lattice packing contacts involving Tyr_{17} and His_{18}, though this possibility is admittedly speculative.

Summary of the Helical Stammer Observed Previously for α/β-Peptide 2

The stammer discontinuity in the crystal structure of α/β-peptide **2** is manifested in a variety of changes in the C-terminal portion of this molecule relative to the C-terminal portion of **1**.[5] Starting at $ACPC_{19}$, the helical conformation of **2** is wound more tightly than that of **1**

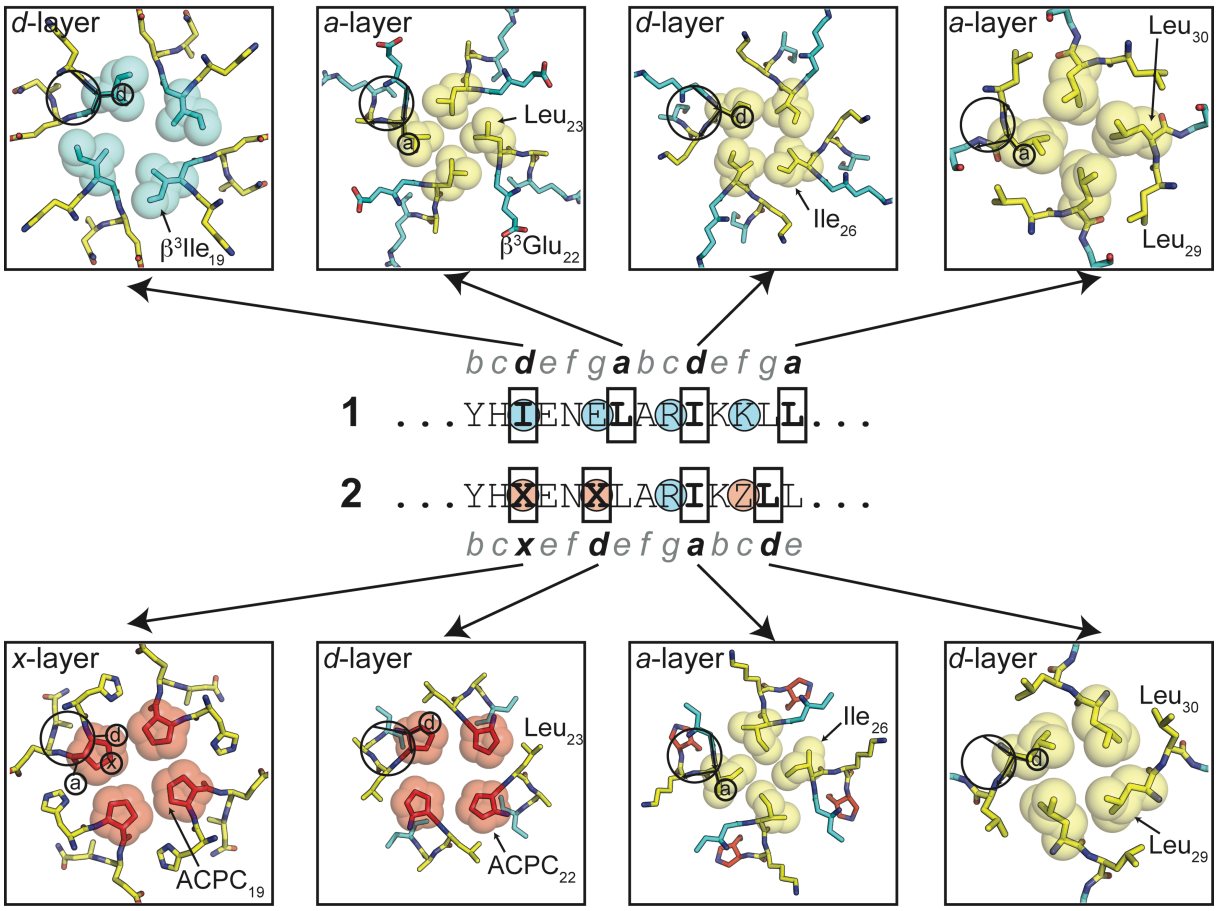

Figure S26. Comparison of the helix-bundles formed by α/β-peptide **1** (PDB: 3C3G), which contains no cyclic β-residues, and α/β-peptide **2** (PDB: 3C3H), which contains six cyclic β-residues (ref. 5). α/β-Peptide **2** suffers from a helical discontinuity near its C-terminus corresponding to a formal deletion of four residues in the heptad. Such discontinuities are designated 'helical stammers' in natural α-peptide helix bundles. The effects of the helical stammer on the structure of **2** are shown in a series of C-terminal hydrophobic core layers from **1** and **2**. In the sequences shown above for **1** and **2**, α-amino acids are abbreviated according to the standard one-letter code. β^3-Residues are highlighted with blue circles and are abbreviated with the single letter that usually represents the corresponding α-amino acid homologue. Cyclic β-residues are highlighted with red circles and are abbreviated as follows: X = ACPC, Z = APC. Hydrophobic core positions (*a*, *d*, and *x*) are shown in bold-face type and are outlined in black boxes. In the core-layer images from the crystal structures, α-amino acids are shown in yellow, β^3-amino acids are shown in blue, and cyclic β-residues are shown in red. The heptad position occupied by the core side-chains is indicated by the overlaid black circles in each image.

(Figure S26). β^3-hIle$_{19}$ packs into a *d*-layer in the hydrophobic core of **1**, but the tighter helical winding causes ACPC$_{19}$ of **2** to occupy a position intermediate between the canonical *d* and *a* heptad positions (a so-called *x*-layer[16]). The effect of the tighter helical winding in the C-terminal portion of **2** becomes even more dramatic one helical turn further along. In **1**,

Leu_{23} packs tightly into the hydrophobic core of the helix-bundle in an *a*-layer. In **2**, however, Leu_{23} has been displaced from the hydrophobic core by $ACPC_{22}$, which packs in a *d*-layer rather than an *a*-layer. The displaced Leu_{23} is relegated to a flanking *e*-position, where it packs against $ACPC_{22}$ in the core but is also partially exposed to solvent. The displacement from the core of Leu_{23} by $ACPC_{22}$ results in a discontinuity in the canonical seven-residue heptad repeat of **2**; the shift of residue 22 to a *d*-position, corresponds to a formal deletion of four residues from the heptad. One helical turn after the stammer, Ile_{26} has shifted from the *d*-position it occupies in **1** to an *a*-position in **2**. Two helical turns after the stammer, Leu_{29} has shifted from the *g*-position it occupies in **1** to a *d*-position in the hydrophobic core of **2**. Leu_{30}, which occupies a core *a*-position in **1**, shifts in **2** to occupy a flanking *e*-position, where it packs against the *d*-position Leu_{29} side-chain.

References

(1) LePlae, P. R.; Umezawa, N.; Lee, H.-S.; Gellman, S. H. *J. Org. Chem.* **2001**, *66*, 5629-5632.
(2) Lee, H.-S.; LePlae, P. R.; Porter, E. A.; Gellman, S. H. *J. Org. Chem.* **2001**, *66*, 3597-3599.
(3) Murray, J. K.; Gellman, S. H. *Org. Lett.* **2005**, *7*, 1517-1520.
(4) Murray, J. K.; Gellman, S. H. *Nat. Protocols* **2007**, *2*, 624-631.
(5) Horne, W. S.; Price, J. L.; Gellman, S. H. *Proc. Natl. Acad. Sci. USA* **2008**, *105*, 9151–9156.
(6) Durchschlag, H.; Zipper, P. *Prog. Colloid Polym. Sci.* **1994**, *94*, 20-39.
(7) 4, C. C. P. N. *Acta Crystallogr. D* **1994**, *50*, 760-763.
(8) McCoy, A. J.; Grosse-Kunstleve, R. W.; Storoni, L. C.; Read, R. J. *Acta Crystallogr. D* **2005**, *61*, 458-464.
(9) Murshudov, G. N.; Vagin, A. A.; Dodson, E. J. *Acta Crystallogr. D* **1997**, *53*, 240-255.
(10) Emsley, P.; Cowtan, K. *Acta Crystallogr. D* **2004**, *60*, 2126-2132.
(11) Lamzin, V. S.; Wilson, K. S. *Acta Crystallogr. D* **1993**, *49*, 129-147.
(12) Kleywegt, G. J.; Jones, T. A. *Structure* **1996**, *4*, 1395–1400.
(13) Ramachandran, G. N.; Sasisekharan, V. *Adv. Protein Chem.* **1968**, *23*, 283–437.
(14) Ramakrishnan, C.; Ramachandran, G. N. *Biophys. J.* **1965**, *5*.

(15) Smith, L. J.; Bolin, K. A.; Schwalbe, H.; MacArthur, M. W.; J.M., T.; Dobson, C. M. *J. Mol. Biol.* **1996**, *255*, 494-506.
(16) Brown, J. H.; Cohen, C.; Parry, D. A. D. *Prot. Struct. Funct. Gen.* **1996**, *26*, 134–145.